THS





# LIBRARY Michigan State University

This is to certify that the

thesis entitled

Structure and Magnetism for Alkali Metal Salts of Nitrogen Heterocyclic Radical Anions

presented by

Eric Keith Meyer

has been accepted towards fulfillment of the requirements for

M.S. degree in <u>Chemistry</u>

Major professor

Date 23 - August - 1999

MSU is an Affirmative Action/Equal Opportunity Institution

O-7639

PLACE IN RETURN BOX to remove this checkout from your record.

TO AVOID FINES return on or before date due.

MAY BE RECALLED with earlier due date if requested.

DATE DUE	DATE DUE	DATE DUE

1/98 c:/CIRC/DateDue.p65-p.14

## STRUCTURE AND MAGNETISM FOR ALKALI METAL SALTS OF NITROGEN HETEROCYCLIC RADICAL ANIONS

Ву

Eric Keith Meyer

### A THESIS

Submitted to
Michigan State University
in partial fulfillment of the requirements
for the degree of

**MASTERS OF SCIENCE** 

Department of Chemistry

1999

### ABSTRACT

## STRUCTURE AND MAGNETISM FOR ALKALI METAL SALTS OF NITROGEN HETEROCYCLES

By

## Eric Keith Meyer

In this thesis we report the magnetic and structural properties of air sensitive radical anion salts Rb\*(2,3-bis-(3-methoxyphenyl) quinoxaline) and M\*(dibenzo[a,c]phenazine) (M = Na, K, Rb). ESR and optical spectroscopy of the complexes in solution revealed insights into ion pairing interactions and spin delocalization. The relationships between structure and magnetism of these salts in the solid state were probed by single crystal X-ray analysis and SQUID. The size of the metal cation dramatically influenced the structural motif of the crystal lattice and the strength of the magnetic coupling between the paramagnetic centers. The larger alkali metals were less solvated in the crystal and provide for greater dimensionality. In fact the Rb\*(Dibenzo[a,c]phenazine) salt crystallized as a solvent free two dimensional network. Although the desired ferromagnetic coupling was not attained in these systems, trends between the strength of the magnetic interactions and the size of the metal were observed.

To My Parents

## **ACKNOWLEDGMENTS**

I would like to thank Dr. Jackson for his assistance and support throughout this research project. I also want to thank members of the Jackson group for their help. I would also like the thank Dr. Andrew Ichimura and Dr. Rui Huang for the assistance they gave me with my research.

I give a special thanks to my parents for their love and encouragement. They motivated me throughout my school years and enforced the value of a good education.

## **TABLE OF CONTENTS**

Chapter 1 Background	1
1.1 Introduction	2
1.2 Magnetic Exchange	3
1.3 Fullerides	13
1.4 Ion Pairing.	14
Chapter 2 Characterization of the Radical Anion Salts in Solution	20
2.1 Introduction	21
2.2 EPR Spectra of the Radical Anions	21
2.3 Optical Spectra of the Radical Anions	24
Chapter 3 Characterization of the Radical Anion Salts in the Solid State	27
3.1 Introduction	28
3.2 X-ray Structure and Magnetism of the Rb <sup>+</sup> (2,3 bis-(3-methoxyphenyl) quinoxaline) <sup>-</sup> (THF) salt	28
3.3 X-ray Structure and magnetism of the Na <sup>+</sup> (dibenzo[a,c]phenazine) <sup>-</sup> (MTHF) <sub>2</sub> salt	32
3.4 X-ray Structure and magnetism of the K <sup>+</sup> (dibenzo[a,c]phenazine) <sup>-</sup> (MTHF) <sub>2/3</sub> salt	37
3.5 X-ray Structure of the Rb <sup>+</sup> (dibenzo[a,c]phenazine) <sup>-</sup> (MTHF) <sub>2/3</sub>	43
3.6 Summary	45

Chapter 4 Experimental	48
4.1 Ligand Synthesis and Purification	49
4.2 Solvent Purification	49
4.3 Synthesis of the Radical Anion Salts	50
4.4 Crystallization of the Radical Anion Salts	51
4.5 X-ray analysis	51
4.6 EPR and ENDOR Analysis	52
4.7 Magnetic Susceptibility Analysis	52
Appendix	53
References	62

## **List of Tables**

Table 2.1	Maximum visible absorbtions for the radical anion salts in THF @ -10°C	25
Table 3.1	Selected Distances and Angles for Rb <sup>+</sup> (2,3 bis-(3-methoxy-phenyl)-quinoxaline) <sup>-</sup> (THF) Salt. Distances are given in Å	30
Table 3.2	Selected Distances and Angles for Na <sup>+</sup> (Dibenzo[a,c]phenazine) <sup>-</sup> (2-MTHF) <sub>2</sub> . Distances are given in Å	35
Table 3.3	Selected Distances and Angles for K <sup>+</sup> (Dibenzo[a,c]phenazine) <sup>-</sup> (MTHF) <sub>2/3</sub> Distances are given in Å	40
Table 3.4	Selected Distances and Angles for Rb <sup>+</sup> (Dibenzo[a,c]phenazine) <sup>-</sup> Distances are given in Å	45
Table 1A	Unit cell parameters and refinement	54
Table 2A	Atomic Coordinates and Isotropic Displacement Parameters for Rb <sup>+</sup> (2,3 bis-(3-methoxyphenyl) quinoxaline)	55
Table 3A	Atomic Coordinates and Isotropic Displacement Parameters for Na <sup>+</sup> (Dibenzo[a,c]phenazine) <sup>-</sup> (MTHF) <sub>2</sub>	56
Table 4A	Atomic Coordinates and Isotropic Displacement Parameters for K <sup>+</sup> (Dibenzo[a,c]phenazine) <sup>-</sup> (MTHF) <sub>2/3</sub>	57
Table 5A	Atomic Coordinates and Isotropic Displacement Parameters for Rb <sup>+</sup> (Dibenzo[a,c]phenazine) <sup>-</sup>	61

## **LIST OF FIGURES**

Figure 1.1	Orbital mixing diagram for 56
Figure 1.2	Spin distribution of [2.2]paracyclophanes incorporating diphenylcarbene units
Figure 1.3	The structure of superconductive K <sub>3</sub> C <sub>60</sub> 14
Figure 1.4	Hyperfine splittings in gauss for the quinoxaline, phenazine, and dibenzo[a,c]phenazine radical anions produced electrochemically19
Figure 2.1	EPR spectra of Na <sup>+</sup> (Dibenzo[a,c]phenazine) <sup>-</sup> in THF recorded at -5°C22
Figure 2.2	(A) EPR spectra of K <sup>+</sup> (Dibenzo[a,c]phenazine) <sup>-</sup> in THF recorded at -96.7°C. (B) ENDOR spectrum of K <sup>+</sup> (Dibenzo[a,c]phenazine) <sup>-</sup> recorded at -96.7°C.
Figure 2.3	Hyperfine coupling constants (in Gauss) from the ENDOR spectrum of K <sup>+</sup> (dibenzo[a,c]phenazine) <sup>-</sup> 24
Figure 2.6	Optical spectra for (a) Rb <sup>+</sup> (2,3 bis-(3-methoxyphenyl) quinoxaline) <sup>-</sup> (B)Na <sup>+</sup> (dibenzo[a,c]phenazine) <sup>-</sup> , and K <sup>+</sup> (dibenzo[a,c]phenazine) <sup>-</sup> (C) Rb+(dibenzo[a,c]phenazine) <sup>-</sup> with and without the presence of C22 cryptand. All optical spectra were done with THF solutions of the radical anion @ -10°C
Figure 3.1	Single crystal X-ray structure of Rb <sup>+</sup> (2,3bis-(3-methoxyphenyl)-quinoxaline) <sup>-</sup> (THF) with atom labeling using atomic symbols. (A) Part of a single chain is shown. (B) Crystal packing for the unit cell looking down the chain axis
	Plot of molar susceptibility $\chi$ vs temperature and $\chi$ t vs temperature for a powder sample of the Rb <sup>+</sup> (2,3 bis-(3-methoxyphenyl) quinoxaline) <sup>-</sup> Salt. The solid line represents a fit to the Curie Weiss Equation for 1-D magnetic coupling
Figure 3.3	Single crystal X-ray structure of Na <sup>+</sup> (Dibenzo[a,c]phenazine) <sup>-</sup> (MTHF) <sub>2</sub> with atom labeling using atomic symbols. (A) A single dimer is displayed. (B) Crystal packing for the unit cell with the shortest distance between dimers depicted by a dashed line. Only seven of twelve dimers in the unit cell are depicted in this figure for clarity

Figure 3.4	Plot of molar susceptibility χ vs temperature and χt vs temperature for a powder sample of the Na <sup>+</sup> (Dibenzo[a,c]phenazine) (2-MTHF) <sub>1/3</sub> salt.					
	The solid line represents a fit to the Bleaney-Bowers equation	37				
Figure 3.5	X-ray structure of K <sup>+</sup> (Dibenzo[a,c]phenazine) <sup>-</sup> (MTHF) <sub>1/3</sub> with atom					
	labeling using atomic symbols. Two repeat units are shown for each					
	chain	39				
Figure 3.6	Plot of molar susceptibility $\chi$ vs temperature and $\chi$ t vs temperature for a powder sample of the K <sup>+</sup> (Dibenzo[a,c]phenazine) <sup>-</sup> (2-MTHF) <sub>1/3</sub> salt.					
	The solid line represents a fit to the Curie Weiss Equation for 1-D					
	magnetic coupling	42				
Figure 3.7	Single crystal X-ray structure of Rb <sup>+</sup> (Dibenzo[a,c]phenazine)- with					
	atom labeling using atomic symbols	43				
Figure 4.1	A modified H cell	50				

## Chapter 1

## Background

1.1	Introduction	2
1.2	Magnetic Exchange	3
1.3	Fullerides	.13
1.4	Ion Pairing	.14

### 1.1 Introduction

In this thesis I report a magnetic and structural analysis for sodium, potassium, and rubidium salts of dibenzo[a,c]phenazine radical anions and the rubidium salt of 2,3 bis-(3-methoxyphenyl) quinoxaline radical anion. Due to the multidisciplinary nature of this work, I will devote chapter 1 to discussing magnetic coupling in pure organic systems and through metal ion bridges. Ion pairing phenomena and their influence on magnetic behavior for alkali metal salts of organic radical anions will also be covered in the first chapter. Chapter 2 will focus on characterization of the salts in solution with EPR and optical spectra being presented. The solid state structural and magnetic properties of the salts will be covered in chapter 3 along with a summary of results and conclusions.

Magnetic materials used for applications such as disk storage, sensors, and switching devices generally consist of metallic centered spin sites assembled into extended networks of at least two dimensions. Only in recent decades has attention been focused on using organic based-paramagnetic units for the construction of magnetic solids. In contrast to metallic magnets which contain d or f orbital spin sites, the spin density of a pure organic magnet is centered on p or s orbitals.

The typical closed shell organic molecule has all its electrons spin-paired in an anti-parallel fashion with all pairs residing in bonding molecular orbitals. In contrast, organic molecules with an odd number of electrons possess excess spin giving rise to a permanent magnetic moment. How the spin density is distributed over the organic framework depends on a number of factors including the presence of conjugation and electronegative heteroatoms.

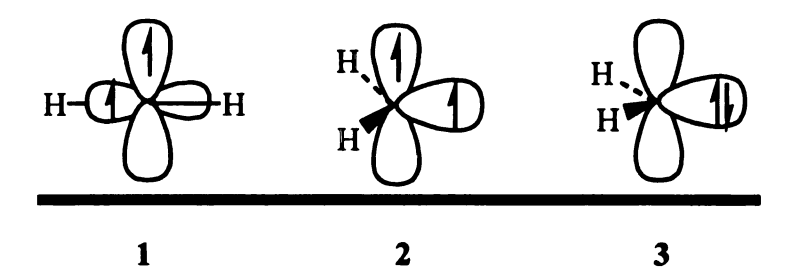
The organic radical centers may interact in an ordered solid array to exhibit either bulk paramagnetic (no interaction), ferromagnetic (spin parallel), or antiferromagnetic coupling (spin pairing). The type of coupling will depend upon how the magnetic orbitals of the molecular fragments overlap in the crystal lattice. A brief overview of magnetic exchange will be given in the next section.

## 1.2 Magnetic Exchange

When two molecular species, each possessing a single unpaired electron, come into contact, they interact in either a high or low spin way. What factors govern the nature and degree of this coupling between paramagnetic subunits? The following discussion will attempt to address this question.

To understand the nature of the exchange interaction between two electrons in two orbitals it is necessary to consider the spatial and spin terms of the total electronic wavefunction. The requirement that the electronic wave function must change sign under the interchange of two opposite sign electrons gives rise to magnetic exchange. It follows that the real space wavefunction must be symmetric for antiferromagnetic coupling and antisymmetric for ferromagnetic coupling. Essentially, an antiferromagnetic interaction can be viewed as a tendency toward the formation of a chemical bond (i.e. electrons paired up in the same orbital), while ferromagnetism is like an antibonding or repulsive interaction between the unpaired electrons. The difference in energy between the two spin states is the exchange energy, 2k, within a fixed orbital framework.

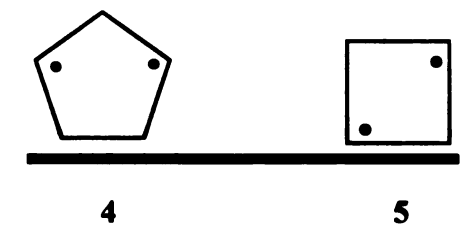
To favor a high spin (ferromagnetically coupled) species where the spins dwell in the same spatial region they must reside in orthogonal orbitals, i.e. the overlap integral between the orbitals must be zero or nearly so.<sup>2</sup> In-phase or bonding interactions resulting from a finite overlap integral will cause a HOMO-LUMO gap favoring a singlet ground state. For a magnetic exchange interaction to exist it is also necessary for the orbitals to be at least partially co-extensive in space. The degree to which the orbitals share the same space is related to the exchange integral. The exchange integral K is evaluated by considering the orbital overlap not taking into account the sign of the MO coefficients. Large overlap leads to destabilizing Coulomb repulsions in the singlet state, but electronelectron repulsion is precluded in the triplet state in accordance with the Pauli Exclusion Principal. The triplet preference for a hypothetical linear carbene 1 where the carbon atom is sp hybridized with two unhybridized p-orbitals underscores this point. To minimize repulsion it is necessary for one electron to reside in each p-orbital, and since these two orbitals are orthogonal the triplet state is favored.



Bending the carbene as in 2 lowers the energy of the p-orbital in the plane of the nuclei by mixing in s-character, while the other p-orbital is not affected.<sup>3</sup> Pairing the electrons into the lower energy orbital is not favored due to the destabilizing electron-electron repulsion and the triplet state is still preferred in the bent form of CH<sub>2</sub>. However

if the energy gap between the orbitals becomes great enough due to further bending, a singlet ground state will be favored as in 3.

Another means of achieving a high spin state between pairs of electrons is superexchange through degenerate orbitals of a closed shell molecule or ion. Although superexchange prevents direct overlap of the SOMO, it does not preclude an exchange interaction. By interacting differently with the half-filled orbitals, the closed shell fragment can shrink the HOMO-LUMO gap and stabilize the triplet ground state. The triplet preference for the biradicals 4 and 5 was explained in these terms.<sup>4</sup> The through-



space interaction of the two radical p-orbitals would lead to a large HOMO-LUMO gap that would favor spin pairing in the lower energy level. However the filled C-H bonding orbitals of the CH<sub>2</sub> subunits can mix with the symmetric HOMO coincidentally raising its energy enough to make it nearly degenerate with the antisymmetric LUMO (shown in Figure 1.1).

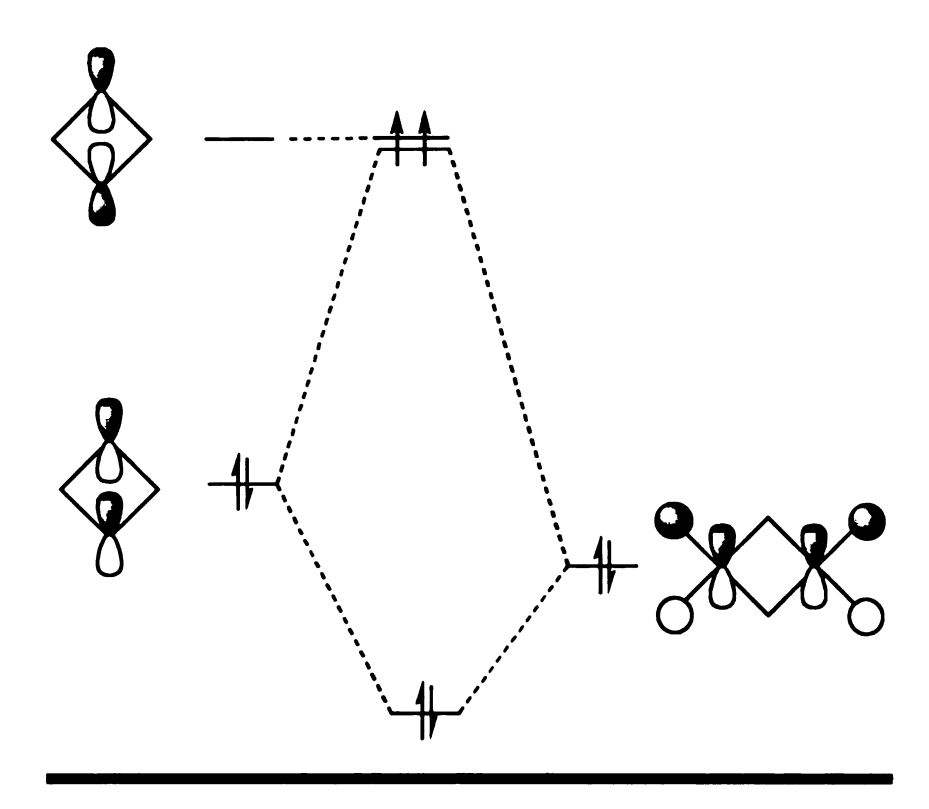


Figure 1.1 Orbital mixing diagram for 5.

Unsaturated organic molecules in which unpaired electrons are delocalized over the  $\pi$  framework fall into a class of molecules referred to as alternant hydrocarbons. A.A Ovchinnikov developed a rather simple method to determine the spin state of planar alternate hydrocarbons by grouping atoms into two sets (labeled + and -) such that no two atoms of the same group are adjacent. By comparing the number of + and - atoms the spin state can be determined. One of the most studied spin coupling units developed in this class of molecules is "metha through a benzene". The biradical for m-xylylene 6 shows a substantial preference for a triplet ground state, although an ionic closed shell resonance structure can be envisioned. In contrast, the p-xylylene biradical displays a singlet ground state.

Incorporation of neutral heteroatoms into the system may not perturb the system enough to change the preference for a triplet state. Placing a nitrogen into the benzene ring as in structure 7 induces only a minimal perturbation of the singlet-triplet gap with the triplet state still favored. However it was recently shown by Dougherty, using computational methods, that meta coupling through a pyridinium ring is antiferromagnetic. From a valence bond perspective 8 has five closed shell resonance structures which lends itself to a singlet ground state. In MO terms the nitrogen cation stabilizes one nonbonding MO with respect to the other, widening the HOMO-LUMO gap. The pyridinium ring 9 is reported to be a ferromagnetic coupling unit since the positively charged nitrogen is placed at a site where the non-bonding molecular orbital coefficients are negligible.

Another class of organic high spin systems are derived from stacking planar paramagnetic  $\pi$  systems. McConnell proposed that high spin coupling would be achieved if  $\pi$  systems pancake such that regions with opposite orbital coefficients overlap. For example, when diphenylcarbene units are incorporated in the [2.2] paracyclophane skeleton the pseudo-ortho and pseudo-para isomers display high spin behavior, while the meta isomer prefers a low spin state. As shown in Figure 1.2 the overlap of the benzene

rings for the ortho and para isomers is out-of-phase, but the meta isomer has an operative in-phase interaction.

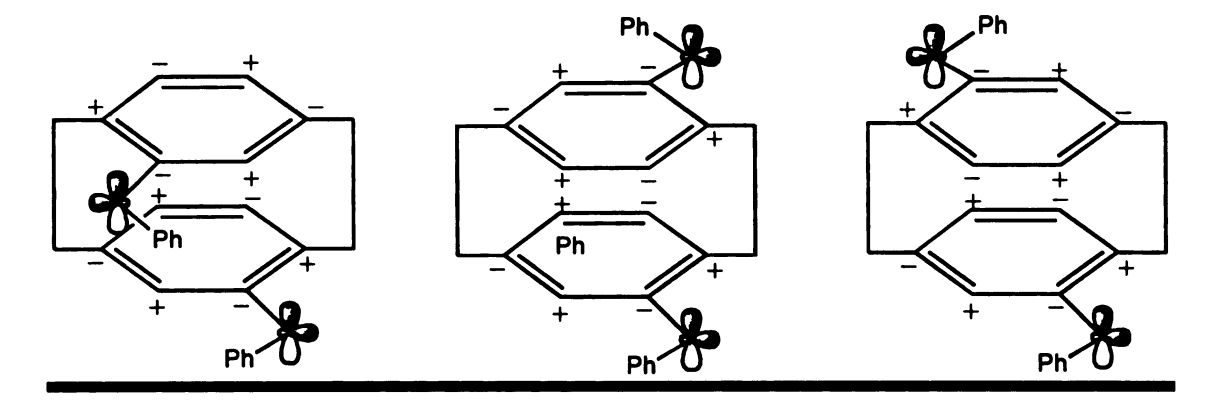


Figure 1.2 Spin distribution of [2.2] paracyclophanes incorporating diphenylcarbene units. The signs of the orbital coefficients in the benzene rings are indicated by +/-.

The major drawback for the development of bulk magnetic materials that apply these systems as coupling units is their high reactivity and poor stability. The search for relatively sTable high spin coupling units that can assemble properly into a crystalline multidimensional magnetic lattice has been difficult. Many organic radicals containing electronegative heteroatoms can be stabilized through complexation to a metal ion. Magnetic exchange through paramagnetic and diamagnetic metal ions will be discussed next.

Formation of bulk magnets through the assembly of organic radicals with oxygen and nitrogen functionalities coordinated to paramagnetic metals has stimulated a lot of interest. Their basic structural units comprise organic radical centers bridged by metal ions and the connectivity must be such that their magnetic orbitals are orthogonal. Unlike conjugated organic radicals with well defined orbital compositions stacked onto one another, the nature of the exchange is less clearly defined for organic radicals

communicating through a metal ion. It is often the nature of the metal-ligand bond that governs the magnetic behavior. For example, with Cu(II) complexes of nitroxyl radicals ferromagnetic exchange is observed when the ligands are coordinated to the  $3d_{z^2}$  orbital of the copper<sup>11c</sup> while antiferromagnetic exchange occurs when the ligand bonds to the  $3d_{xy}$  orbitals.<sup>11a</sup> Ryza Musin proposed that a slight delocalization of the electron from the  $\pi^*$  orbital of the nitroxide group to the  $3d_{z^2}$  orbital of the paramagnetic Cu(II) ion is responsible for the magnetic coupling.<sup>12</sup>

The ability of diamagnetic ions to mediate exchange interactions between organic radicals via their empty and occupied orbitals has only been recently documented. As with paramagnetic bridges, the nature of the magnetic coupling is governed by the metalligand interaction. A number of novel systems possessing strong exchange interactions have been developed using diamagnetic metal bridges. Complexation of quinone radicals to zinc, reported by BuíLock and Harley-Mason in 1951, is one of the earliest examples of a radical organic ligand coordination to a diamagnetic metal ion.<sup>13</sup> Pierpont and coworkers have discovered a series of high spin octahedral complexes consisting of paramagnetic semiquinone ligands chelated to a variety of transition metals.<sup>14</sup> The metal orbital interacting with the semiquinone  $\pi^*$  molecular orbital often determines the spin state for these systems. For instance, Ga(III) and Al(III) metals chelating three 3,6-ditert-butyl-1,2-semiquinoate (DBSQ) radical anions possess an S=3/2 ground state while the analogous Co(III) trimer displays weak antiferromagnetic exchange. The ferromagnetic coupling for the Ga(III) and Al(III) trimers originates in the interaction of an empty metal p-orbital with the semiquinone  $\pi^*$  orbital. For the Co(III) complex

coupling through the filled metal  $3d\pi$  orbital is operative. A similar coupling mechanism is responsible for the near diamagnetism of the square planar M(II) (SQ)<sub>2</sub> where M=Ni, Pd, Pt and SQ = 3,5-DBSQ, 3,6-DBSQ where filled metal d-orbitals and semiquinone  $\pi^*$  orbitals are interacting.<sup>15</sup> These results demonstrate the dependence of the exchange interaction upon the electronic configuration of the diamagnetic ion.

High spin complexes  $M^{2*}(1,4\text{-di-tert-butyl-1,4-diazabutadiene})_2$ , where M=Mg, Zn, provide other prominent examples of magnetic coupling through a diamagnetic metal. In these systems the two diazabutadiene units complex to the divalent metal and are orthogonal to one another. Biradical 10 has one electron delocalized on each  $N_2C_2$  backbone; providing the proper motif for a high spin complex. In contrast, the analogous Ga(III) and Al(III) species 11 has one ligand behaving as a dianion and the other as a singly reduced radical anion, yielding only a doublet ESR signal. For biradical 10 an equilibrium between the dipole-dipole coupled species and the ionic monoradicals was proposed by the authors to explain the loss of high spin coupling at room temperature. Internal disproportionation of this nature can provide a challenge for the design of bulk ferromagnetic materials from these materials, especially if the diradical centers come into close proximity in the crystalline lattice.

t-Bu

t-Bu

t-Bu

t-Bu

t-Bu

t-Bu

N

t-Bu

N

M

$$t$$
-Bu

 $t$ 

The research presented in this thesis focuses on assembling magnetic materials by connecting organic paramagnetic centers through alkali metal cation linkages. A few novel magnetic systems have been developed using this strategy. Alkali metal salts of fluorenone, which have been shown to self assemble into ion pairs, provide the earliest examples of high spin coupling through alkali metal ions. Hiroto's proposal that the fluorenone radicals are linked through a Na<sup>+</sup><sub>2</sub> O<sub>6</sub><sup>-</sup><sub>2</sub> parallelogram<sup>17</sup> was later supported by the X-ray analysis of a [fluorenone<sup>-</sup>][Na<sup>+</sup>(dme)<sub>2</sub>]<sub>2</sub> crystal by Bock. <sup>18</sup> The Na<sup>+</sup> ion is solvated by two DME molecules allowing for chelation to only two fluorenone oxygens in order to achieve its preferable coordination sphere of six. The triplet benzophenone

salt 12 is thought to possess a similar dimeric structure. It is interesting to note the absence of magnetic susceptibility data on these salts, but long range order may be precluded due to the large dimer-dimer distances. Ion pairing of alkali metal cations and

organic radical anions is an important concept that will be discussed in the following section.

Further insights into magnetic coupling through alkali metal cations were developed from work done in this lab. Using lithium and sodium salts to bring neutral paramagnetic tripod ethers 13 into communication was largely unsuccessful.<sup>19</sup> It was postulated that the large metal-ligand distance contributed to the weak coupling.

13

A more successful approach was to chelate radical anion centers to alkali metal cations in an attempt to strengthen the interaction between the paramagnetic centers through stronger electrostatic interactions. Bulk one dimensional ferromagnetism was reported by Misiolek and Jackson for crystals of the 4-Carboxy-TEMPO radical sodium salt.<sup>20</sup> Coupling between the TEMPO radicals mediated by sodium cations were apparently responsible for the materials magnetic behavior. The potassium salt also was reported to display ferromagnetic behavior. Weak antiferromagnetic coupling along chains of K<sup>+</sup>[2,3-Bis(2-pyridyl)quinoxaline] (THF)<sub>2</sub> radical anion salt was also reported by Dye and Jackson.<sup>21</sup> Multidimensional coupling is precluded in this systems due to the

large gaps between the chains. These results encouraged the development of other similar systems where alkali metal cations would provide an exchange coupling pathway.

### 1.3 Fullerides

It has been demonstrated that  $C_{60}$  and  $C_{70}$  doped with alkali metals are conductive and that superconductivity has been observed in  $K_3C_{60}$  and  $Rb_3C_{60}$  at low temperature<sup>22</sup>.  $K_3C_{60}$  possesses a Tc value of 19.3K, but the heavily doped  $K_6C_{60}$  phase is not superconductive.<sup>23</sup> Diffraction data reported by P.W. Stephens of  $K_3C_{60}$  showed that the potassium atoms reside in tetrahedral and octahedral sites within the  $C_{60}$  lattice (Figure 1.3).<sup>24</sup> This composition has also been identified as the metallic phase, however new compositions have been reported with possessing higher superconducting transition temperatues.<sup>25-27</sup> Some distortion of the  $C_{60}$  framework in comparison to the neutral species is observed, but the spacing between the  $\pi$  systems remains nearly the same. The shortest distance between a potassium ion and a  $C_{60}$  carbon atom is 3.27A as compared to 3.06A in intercalated graphite. It is proposed that the conductivity of this salts arise from the delocalization of one electron per metal into a conduction band consisting of three degenerate orbitals.

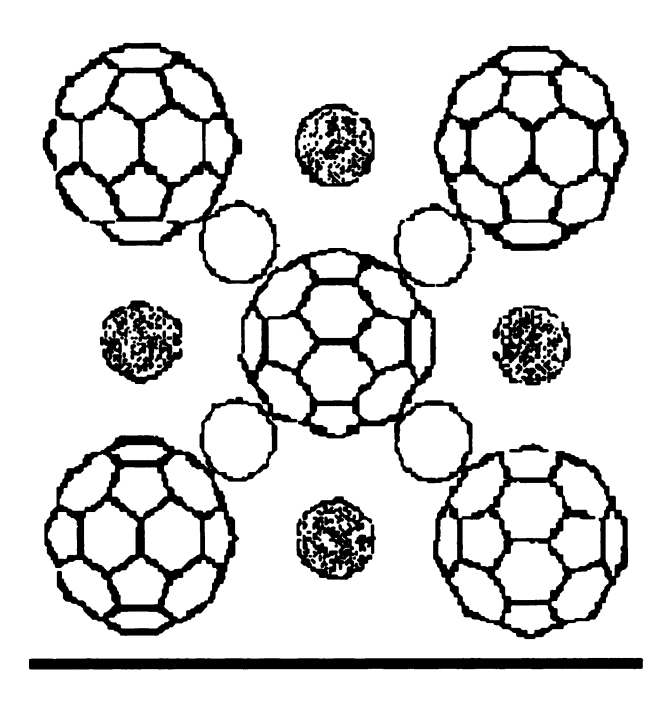


Figure 1.3 The structure of superconductive  $K_3C_{60}$ . The shaded and white circles represent octahedral and tetrahedral sites respectively.

## 1.4 Ion Pairing

The magnetic properties of alkali metal salts of organic anions in solution and in the solid state can be influenced by how strongly the metal associates with the radical anion. For the design of magnetic solids it is desirable to achieve tight ion pairing between the metal and the organic radical center. Factors such as solvent polarity, cation size, and the degree of localization of charge density on the organic unit all play a role influencing the tight ion pair-solvent separated ion pair equilibrium. EPR has been effectively used to elucidate alkali metal organic anion interactions in solution. In systems where the metal comes into close proximity to the organic anion some leakage of spin density onto the metal can occur, provided an orbital pathway exists. Spin delocalization onto the cation is indicated by the presence of alkali metal coupling constants in the EPR spectrum.

Unsaturated organic ring systems reduced with alkali metal often display small metal splittings. Weissman reported the first  $^{23}$ Na coupling constant for a THF solution of the naphthalene radical anion salt due to spin transfer from the naphthalene  $\pi$ -system to the sodium s orbital. A sodium splitting of 1.05 gauss was observed at room temperature and declined steadily with decreasing temperature. From this initial study it was postulated that the equilibrium between tight ion pairs and solvent separated ones is temperature dependent.

The presence of heteroatoms on the organic moiety can lead to tight ion pairing in solution resulting in large metal coupling constants. The sodium splitting for odimesitoylbenzene radical anion is 6.95gauss in DME at room temperature, one of the largest reported. These ion pairs are considered "tight" while alkali metal cations associating with hydrocarbon radical anions are often defined as "loose". Ether solvents such as THF or glymes can effectively compete for the metals coordination sphere since the charge on unsaturated hydrocarbons tends to be more delocalized then on molecules possessing electronegative heteroatoms.

The unusually large alkali metal coupling constants a(<sup>39</sup>K)=1.2-1.5, a(<sup>85</sup>Rb)=0.4-0.84, a(<sup>87</sup>Rb)=14-28, and a(<sup>133</sup>Cs)=7.0-26 gauss reported by Gerson for salts of 1,4 and 2,3 di-tert-butylbuta-1,3 dienes in DME and THF provides an interesting anomaly.<sup>30</sup> It is rationalized by Gerson that partial encapsulation of the metal by t-butyl groups prevents metal solvolysis and facilitates tight ion pairing. Molecular modeling seems to support this hypothesis.

Metal splittings of aromatic nitrogen heterocyclic radical anions often do not appear in the EPR spectrum although contact ion pairing does occur in these systems. No

metal splittings were reported for the sodium and potassium salts of diphenylquinoxaline<sup>31</sup> (compound 14) in DME and the potassium salt of 2,3-Bis(2-Pyridyl)quinoxaline<sup>21</sup> (compound 15) in THF. Chelation to the nitrogen lone pair places the metal s-orbital in the nodal plane of the  $\pi$  system in the diphenylquinoxaline species preventing a pathway for spin transfer.

Often the degree of ion pairing in solution can have a large impact on the assembly in the crystalline lattice since solvent molecules can compete effectively for the coordination sphere of the metal. In recent years a number of investigations done on alkali metal salts of unsaturated ring systems by Bock and co-workers has uncovered clues in cation solvation and aggregation phenomena of these species in the crystal lattice. He recently made this general conclusion, He comparison of single crystal structure data with results from NMR, ESR, or UV/vis measurements, it often becomes obvious that solid state structures of organometallic complexes largely represent the species in solution." The crystallization process of alkali metal cations and organic anions into a lattice can be controlled by a number of factors among which solvation can play a dominating role. Crystallizing from highly chelating environments often result in solvent

wrapped cations, only weakly coordinated to the anion. A dramatic example is the crystallization of potassium perylene radical anion in triglyme. The potassium metal is encapsulated in a shell of two triglyme molecules completely separated from the perylene anion. Extensive delocalization of negative charge around this unsaturated  $\pi$  hydrocarbon seems to further compromise contact ion pair formation. Solvation of the metal to this extent is undesirable from a magnetic standpoint since the orbitals of isolated organic anions and metal cations will not overlap significantly.

Since the solvation energies of alkali metal cations tend to decrease with increasing ionic radii the larger metals tend to chelate less solvent, leaving more sites available for radical anion ligands to coordinate. This trend is displayed quite dramatically with alkali metal salts of [TCNE] radical anions.

Crystal structures of [TCNE]<sup>-</sup> M<sup>+</sup> complexes where M = Na, K, and CS have been reported by Bock and co-workers.<sup>34</sup> The cesium tetracyanoethylenide salt crystallizes from DME and hexane into a solvent free 2-D network. Although DME is an energetically favorable ligand for cation solvation, its "bite" is too small for both oxygens to properly coordinate to the cesium cation with an ionic radii of 169pm. The result is two unique cesium ions coordinated to seven and eight nitrogen centers. TCNE radical anions stack into chains with Cs<sup>+</sup> connecting the chains and adjacent ligands. Solvent free networks possessing small ligand-ligand distances are desirable synthetic targets due to their potential magnetic properties.

In contrast to the cesium structure, the sodium and potassium salts possess a single DME chelated to the metal. The structural motifs of the chains are also influenced

by the size of the cation. The lattice of the sodium salt consists of  $\pi$  stacked dimers separated by 300 pm and connected by a DME chelated Na<sup>+</sup> ion forming infinite chains. The potassium structure has layers of TCNE ions separated by 315 and 360pm with the cations residing in the smaller gap.

Recently crystals were grown using substituted quinoxalines as the radical anion center. The facilitation of contact ion pair formation through the concentration of negative charge at the two nitrogen atoms makes them attractive for building multidimensional magnetic networks. Crystals of sodium and potassium salts of diphenyl quinoxaline in glyme assemble into one dimensional chains with the metal cations coordinated directly to the nitrogen lone pair forming M<sup>+</sup>(solvent) bridges linking the anions.<sup>31</sup> Interestingly no temperature dependent susceptibility data was reported for the salt. The sodium and potassium salts are rather similar considering the 36pm difference in their atomic radii. The potassium salts of Bis(2-Pyridyl)quinoxaline provide a prominent example of how metal solvation can influence the dimensionality of the crystal lattice. Crystallizing in THF resulted in one dimensional chains of the quinoxaline connected by K<sup>+</sup>(THF)<sub>2</sub> linkages while in methylamine dimers resulted from three solvent molecules coordinating to the metal.<sup>21</sup> Presumably the stronger chelating ability of the amine nitrogen and its smaller size makes it better able to compete for the potassium coordination sphere then THF.

Many aromatic nitrogen heterocyclic radical anions have been characterized in solution, but not in the solid state. EPR analysis of quinoxaline, phenazine and dibenzo[a,c]phenazine radical anions along with molecular orbital calculations indicate that the spin density distribution is fairly localized on the nitrogen atoms.<sup>35</sup> The proton

and nitrogen hyperfine splitting constants of many other nitrogen heterocyclic radical anions have also been measured (Figure 1.4).

$$\begin{bmatrix} 1.40 & 2.22 & 5.76 \\ N & 3.27 \end{bmatrix} \begin{bmatrix} 1.51 & 1.80 & 5.14 \\ N & N & N \end{bmatrix} \begin{bmatrix} 1.78 & 4.95 \\ 1.46 & N & N \end{bmatrix}$$

Figure 1.4 Hyperfine splittings in gauss for the quinoxaline, phenazine, and dibenzo[a,c]phenazine radical anions produced electrochemically in DMF with tetra-n-butylammonium iodide as a supporting electrolyte.

## Chapter 2

Characterization	of t	he I	Radical	Anion	Salts	in	<b>Solution</b>
------------------	------	------	---------	-------	-------	----	-----------------

2.1	Introduction	21
2.2	EPR Spectra of the Radical Anions	21
2.3	Optical Spectra of the Radical Anions	.24

### 2.1 Introduction.

In this chapter I will report the EPR spectrum for the sodium and potassium salts of the dibenzo[a,c]phenazine radical anion. The hyperfine splitting constants that I report are taken directly from the ENDOR spectrum of the potassium salt. In the last section of this chapter I will show optical spectra for THF solutions of Rb<sup>+</sup> ((Bis-2-methoxyphenyl) quinoxaline) and M<sup>+</sup> (dibenzo[a,c]phenazine) (M = Na, K, Rb) and make comparisons to spectra of other anion salts reported in literature. The influence ion pairing has on the optical spectrum of these salts in solution will be discussed.

## 2.2 EPR and ENDOR Spectra of the Radical Anions.

The solution EPR spectrum for the Na<sup>+</sup>(Dibenzo[a,c]phenazine) salt in THF is displayed in Figure 2.1 and solution EPR and ENDOR spectra for the potassium salt are in Figure 2.2. Due to the complexity of the hyperfine splitting, the coupling constants shown in Figure 2.3 were taken directly from the ENDOR spectrum by Andrew Ichimura. Inspection of the Figure reveals that the center of the spectrum is split by the sodium cation. It is possible that in the lowest energy state of the complex the cation resides directly over the π system. Chelation to the nitrogen lone pair may be energetically disfavored due to steric congestion caused by the hydrogen atom on the phenanthrene subunit. In the EPR spectrum of Na<sup>+</sup>(2,3-diphenylquinoxaline) in dimethoxyethane reported by Bock, metal splitting was not reported. In this cas,e the rotation of the phenyl rings can allow the sodium to chelate directly to the nitrogen lone pair minimizing spin transfer. Dimethoxyethane may also solvate the metal weakening the association

between the cation and radical anion. No metal splitting appears in the EPR spectrum for the potassium salt.

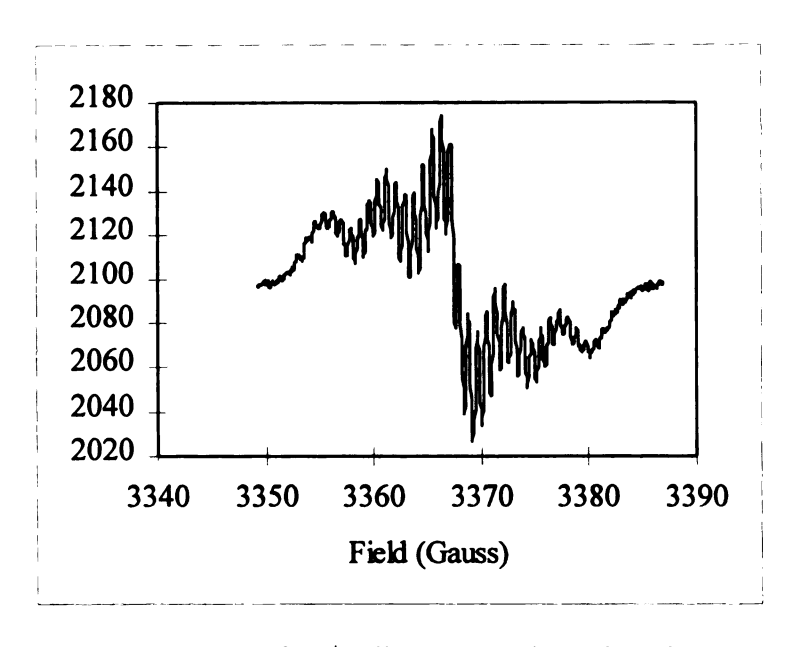
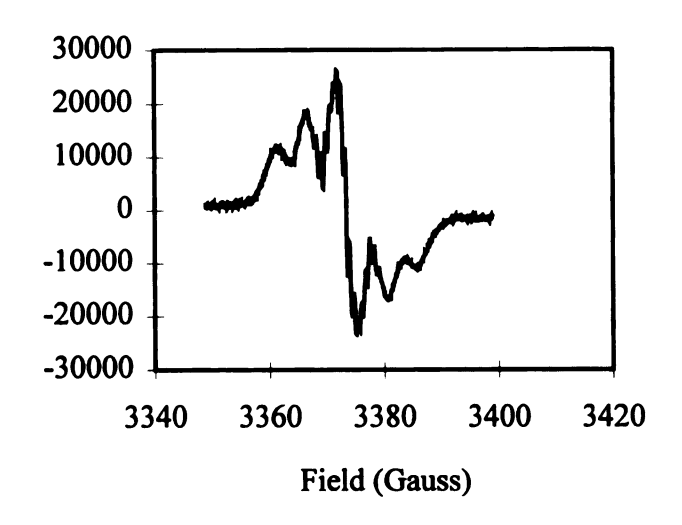


Figure 2.1 EPR spectra of Na<sup>+</sup>(Dibenzo[a,c]phenazine)<sup>-</sup> in THF, recorded at -5°C.



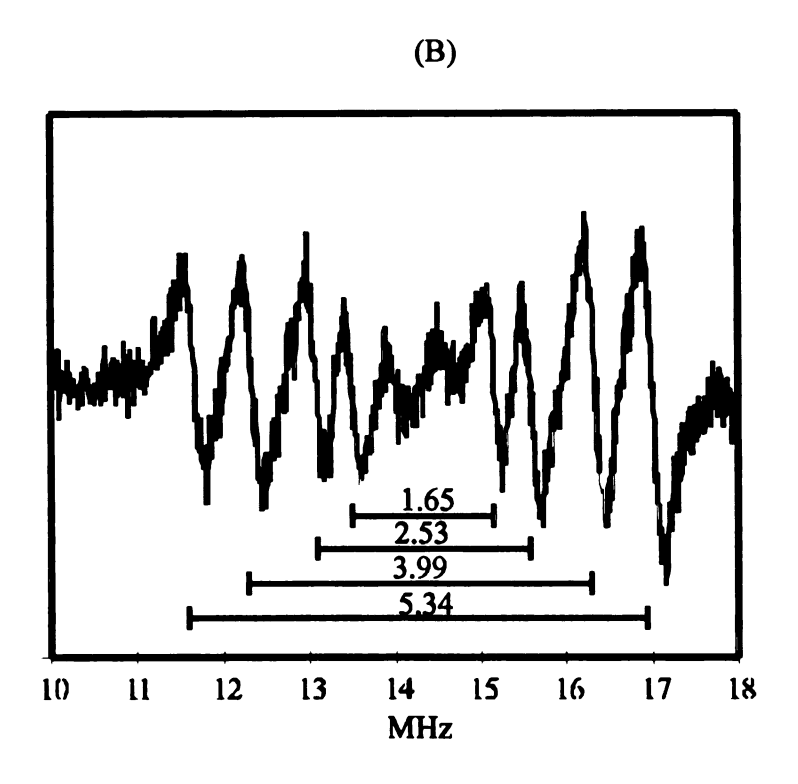


Figure 2.2 (A) EPR spectra of K<sup>+</sup>(Dibenzo[a,c]phenazine) in THF, recorded at -96.7°C. (B) ENDOR spectrum of K<sup>+</sup>(Dibenzo[a,c]phenazine) , recorded at -96.7°C.

Figure 2.3 Hyperfine coupling constants (in Gauss) from the ENDOR spectrum of  $K^{+}(dibenzo[a,c]phenazine)^{-}$ 

## 2.3 Optical Spectra of the Radical Anions.

The optical spectrum of the radical anion salts in THF (Figure 2.4) were measured in the range 400-2000nm. Two visible absorptions were observed for all the salts along with a broad band in the near IR. The spectrum for the intensely blue Rb<sup>+</sup> (2,3 bis-(3methoxyphenyl) quinoxaline) has two visible absorptions at 550nm and 620nm and one broad band in the near IR centered around 1100nm. The spectrums for red THF solutions of the dibenzo[a,c]phenazine radical anions are shown in Figure 2(b) and 2(c). The optical spectrum reveals a sharp absorption in the 558 to 568nm range; the exact position depends on the size of the alkali metal cation (Table 2.2). Similar bathochromic shifts arising from ion pairing have been reported for alkali metal salts of various aromatic hydrocarbon radical anions and ketones in solution.<sup>38, 39</sup> These studies suggested that the shifts to higher wavelengths are a result of a weaker ion pair between the radical anions and the larger alkali metal cations. The shorter wavelength visible absorption was unaffected by the size of the cation and may indicate the presence of aggregates or a different species.

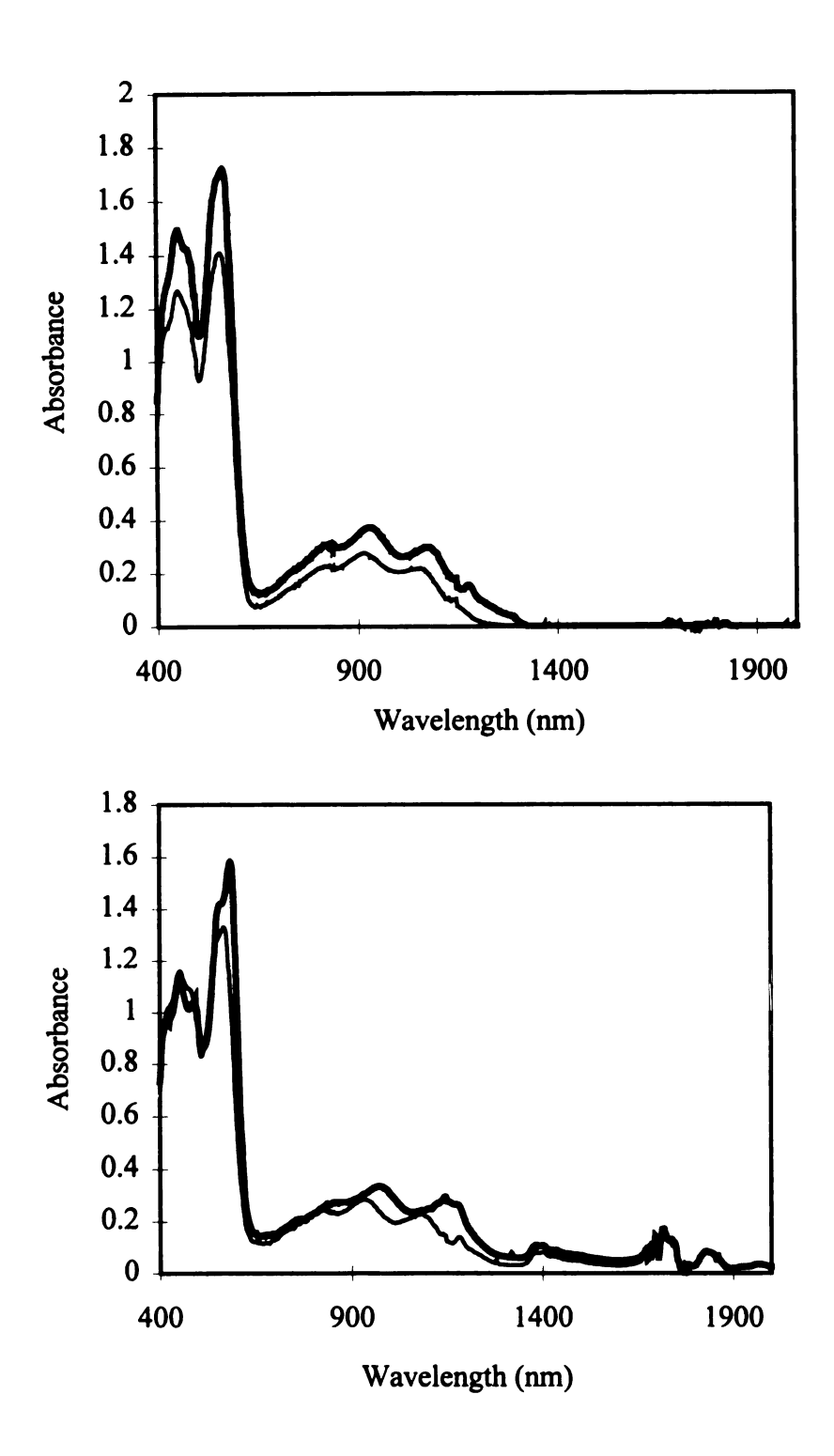


Figure 2.4 (Top graph) Optical spectra for Na<sup>+</sup>(dibenzo[a,c]phenazine)<sup>-</sup> (dark line), and K<sup>+</sup>(dibenzo[a,c]phenazine)<sup>-</sup> (light line). (Bottom graph) Rb<sup>+</sup>(dibenzo[a,c]phenazine)<sup>-</sup> with (dark line) and without the presence of C222 cryptand (light line).

To further weaken the interaction between the metal and radical anion C22 cryptand was introduced into the rubidium salt solution. The result is the formation of a cryptand separated ion pair where the interactions between the anion and metal cation are significantly reduced (Figure 2.5). As expected the adsorption peak was red shifted significantly (568nm to 584nm).

$$\begin{bmatrix} N & Cryptand [2.2.2] \end{bmatrix} \begin{bmatrix} N & Cryptand [2.2.2] \end{bmatrix} \begin{bmatrix} N & Rb^{+} & N \\ N & Rb^{+} & N \end{bmatrix}$$

Figure 2.5 Formation of the Rb<sup>+</sup> C22 cryptand separated ion pair.

# Chapter 3

Characterization of the Radical Anion Salts in the Sol
--

3.1	Introduction	28
3.2	X-ray Structure and Magnetism of the Rb <sup>+</sup> (2,3 bis-(3-methoxyphenyl) quinoxaline) <sup>-</sup> (THF) salt	28
3.3	X-ray Structure and magnetism of the Na <sup>+</sup> (dibenzo[a,c]phenazine) (MTHF) <sub>2</sub> salt	32
	X-ray Structure and magnetism of the K <sup>+</sup> (dibenzo[a,c]phenazine) <sup>-</sup> (MTHF) <sub>2</sub> salt	37
3.5	X-ray Structure and magnetism of the Rb <sup>+</sup> (dibenzo[a,c]phenazine) <sup>-</sup> salt	43
3.6	Summary	45

#### 3.1 Introduction.

In this chapter I will report the single crystal X-ray structures and solid state susceptibility data for Rb \*(2,3 bis-(3-methoxyphenyl) quinoxaline) (THF),

Na\*(dibenzo[a,c]phenazine) (MTHF)<sub>2</sub>, K\*(dibenzo[a,c]phenazine) (MTHF)<sub>23</sub>, and

Rb\*(Dibenzo[a,c]phenazine) salts. The extremely air sensitive crystals were prepared by diffusing pentane into THF or MTHF solutions of the radical anion salt at room temperature under high vacuum. Since they were grown under comparable conditions the structural diversity observed with these salts can be attributed to the size of the alkali metal cation. The magnetic data provides further insight into structure-magnetic relationships of organic radical anions bridged by diamagnetic alkali metal cations.

Tables of selected distances and angles will be presented for each structure. A

Table summarizing unit cell dimensions and refinement is located at the beginning of the appendix. The coordinate Tables are also in the appendix.

# 3.2 X-ray Structure and Magnetism of the Rb<sup>+</sup>(2,3 bis-(3-methoxyphenyl) quinoxaline)<sup>-</sup> (THF) Salt.

The Rb<sup>+</sup>(2,3 bis-(3-methoxyphenyl) quinoxaline) (THF) salt crystallizes into polymeric chains of 2,3 bis-(3-methoxyphenyl) quinoxaline radical anions strung together by N<sup>5</sup>-Rb<sup>+</sup>-N<sup>5</sup> linkages. The chains possess a connectivity pattern of repeating N<sup>5</sup>-Rb<sup>+</sup>-N<sup>5</sup>-(C-C)<sub>2</sub>-N<sup>5</sup>-Rb<sup>+</sup> rings (Figure 3.1a) with Rb-N-Rb bond angles of 117°. The radical anions stack parallel to one another along the C direction with singly THF solvated Rb<sup>+</sup> ions residing between them. Within each chain the ligands point in the same direction

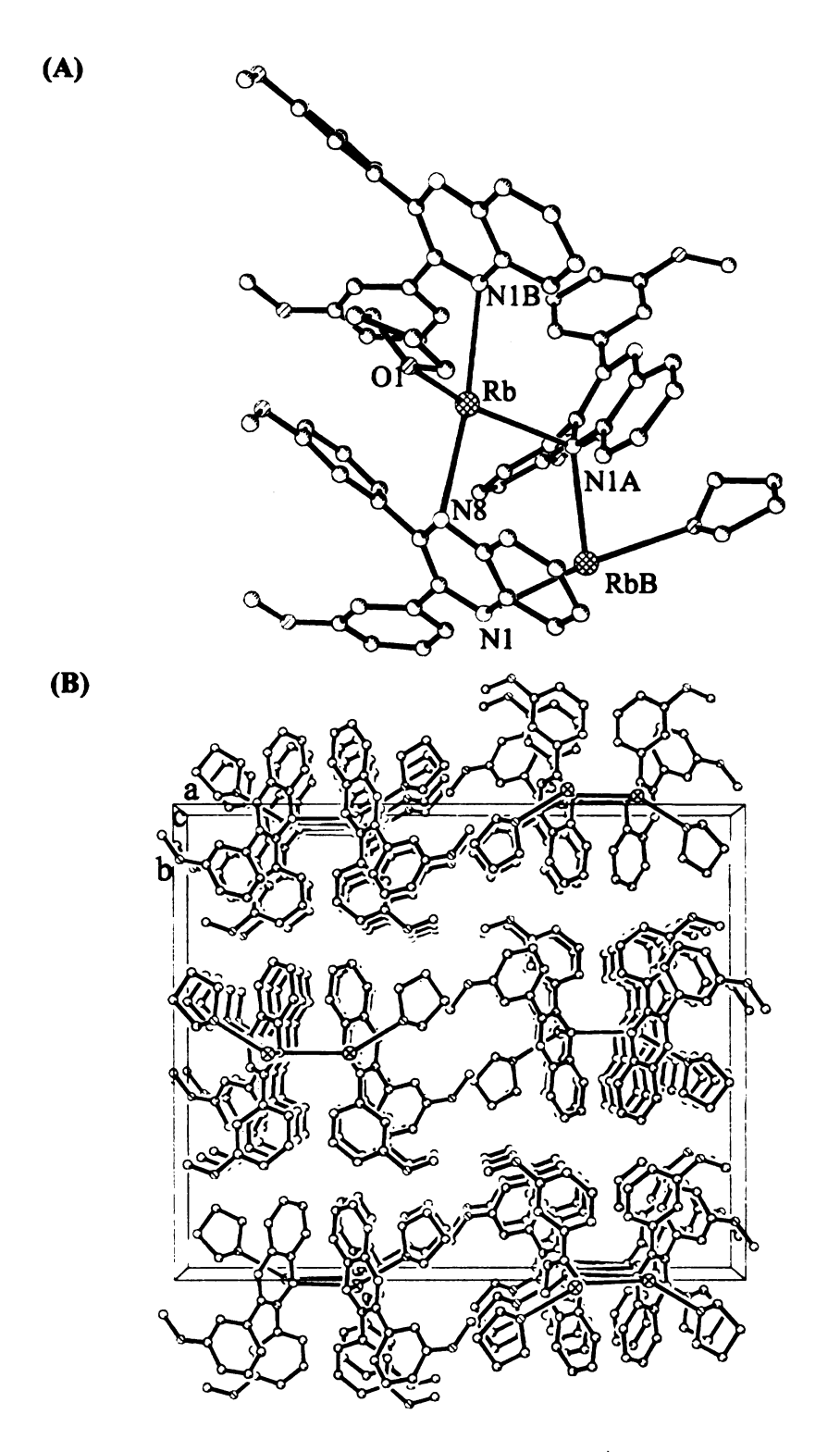


Figure 3.1 Single crystal X-ray structure of Rb<sup>+</sup>(2,3-bis-(3-methoxyphenyl)quinoxaline) (THF) with atom labeling using atomic symbols. (A) Part of a single chain is shown. (B) Crystal packing for the unit cell looking down the chain axis.

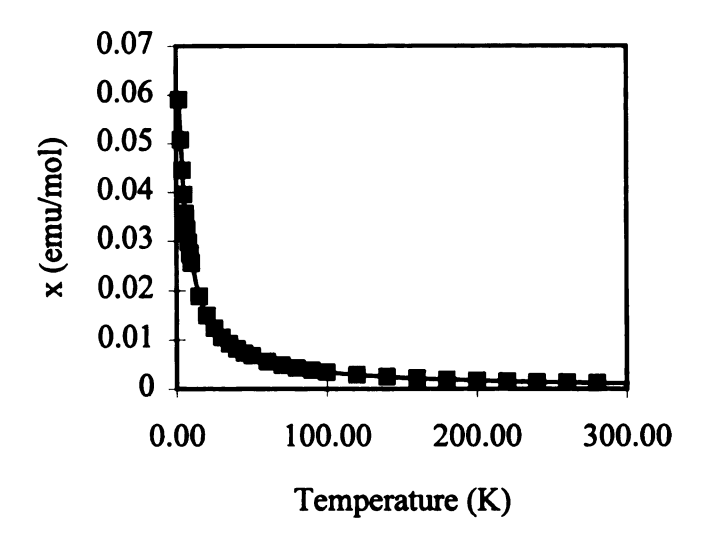
along the stacking axis, presumably to optimize packing. The phenyl rings are twisted 39.7° and 45.3° from the plane of the quinoxaline moiety. Selected angles and distances are displayed in Table 3.1.

Three nitrogens and one THF oxygen form a distorted square planar environment around the metal with an average Rb-N distance of 3.1 Å. A formally seven fold coordination sphere of the cation is completed through contacts under 3.5 Å to two adjacent carbon centers on the phenyl ring C(9), C(10) and one carbon adjacent to the nitrogen on the quinoxaline moity C(2B). The methoxyphenyl ring (C10B-C18B) caps off one face of the cation but does not appear itself to be close enough to interact. It is interesting to note that the methoxy oxygen does not serve as a ligand in the environment of the metal.

**Table 3.1** Selected Distances and Angles for Rb<sup>+</sup>(2,3 bis-(3-methoxyphenyl) quinoxaline) (THF) Salt. Distances are given in Å.

Distances			
Rb-N(1A)	3.212(2)	N(1)-Rb-C(10)	103.14(5)
Rb-O(1)	2.885(2)	O(1)-Rb- $C(2B)$	126.88(6)
Rb-N(1B)	2.973(2)	N(1)-Rb-C(2B)	93.13(5)
Rb-N(8)	3.042(2)	N(8)-Rb-C(2B)	95.66(5)
Rb-C(10)	3.306(2)	N(1)-Rb-C(2B)	23.71(5)
Rb-C(2B)	3.438(2)	C(10)-Rb- $C(2B)$	121.02(5)
Rb-C(9)	3.462(2)	O(1)-Rb- $C(9)$	98.06(5)
Rb-C(11)	3.540(2)	N(1B)-Rb-C(9)	165.89(5)
		N(8)-Rb-C(9)	23.08(5)
Angles		N(1A)-Rb-C(9)	88.00(5)
O(1)-Rb-N(1B)	77.50(5)	C(10)-Rb- $C(9)$	25.41(5)
O(1)-Rb-N(8)	82.87(5)	O(1)-Rb- $C(11)$	72.04(6)
N(1B)-Rb-N(8)	160.01(5)	N(1B)-Rb-C(11)	124.50(5)
O(1)-Rb-N(1A)	149.85(5)	N(8)-Rb-C(11)	50.60(5)
N(1A)-Rb-N(1B)	102.59(4)	N(1B)-Rb-C(11)	126.51(5)
N(8)-Rb-N(1A)	92.47(5)	C(10)-Rb- $C(11)$	23.48(5)
O(1)-Rb- $C(10)$	94.10(6)	C(9)-Rb-C(11)	42.00(5)
N(1)-Rb-C(10)	140.69(5)	O(101)-Rb- $C(3B)$	109.23(6)
N(8)-Rb-C(10)	44.04(5)	Rb-N(1)-Rb(B)	116.81(5)

Magnetic susceptibility data for the crystalline salt was recorded over the temperature range 2-300K. The χt vs t plot is displayed in Figure 3.2 along with a fit to the one dimensional Curie-Weiss model for magnetic coupling. The Weiss constant for the salt is found to be -4K indicating antiferromagnetic behavior at low temperature. The Curie constant is 0.35emu/mol which is slightly lower then the expected value of 0.375emu/mol for a crystal of single spin molecules. Some decomposition of the extremely air sensitive crystals may be responsible. The magnetism appears to be consistent with the structural information just presented. The weak magnetic interaction is a consequence of the nearly 5 Å distance between the paramagnetic centers and the poor ability of the Rb<sup>+</sup> to act as a coupling unit. Long range magnetic exchange throughout the crystal lattice is precluded by the large chain-chain distances.



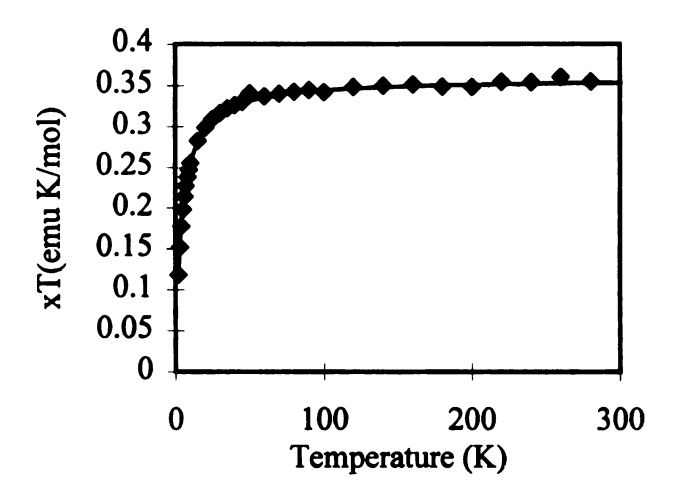


Figure 3.2 Plot of molar susceptibility  $\chi$  vs temperature and  $\chi$ t vs temperature for a powder sample of the Rb<sup>+</sup>(2,3 bis-(3-methoxyphenyl) quinoxaline)<sup>-</sup> Salt. The solid line represents a fit to the Curie Weiss Equation for 1-D magnetic coupling.

# 3.3 X-ray Structure and magnetism of the Na<sup>+</sup>(Dibenzo[a,c]phenazine)<sup>-</sup> (MTHF)<sub>2</sub> salt.

The Na<sup>+</sup>(Dibenzo[a,c]phenazine)<sup>-</sup> (MTHF)<sub>2</sub> salt crystallizes into an orthorhombic unit cell of cyclic dimers possessing a Na<sup>+</sup>-N<sup>δ</sup>(C-C)<sub>2</sub><sup>-</sup>-N<sup>δ</sup>-Na<sup>+</sup> connectivity pattern (Figure 3.2). Selected distances and angles with deviations are displayed in Table 3.2.

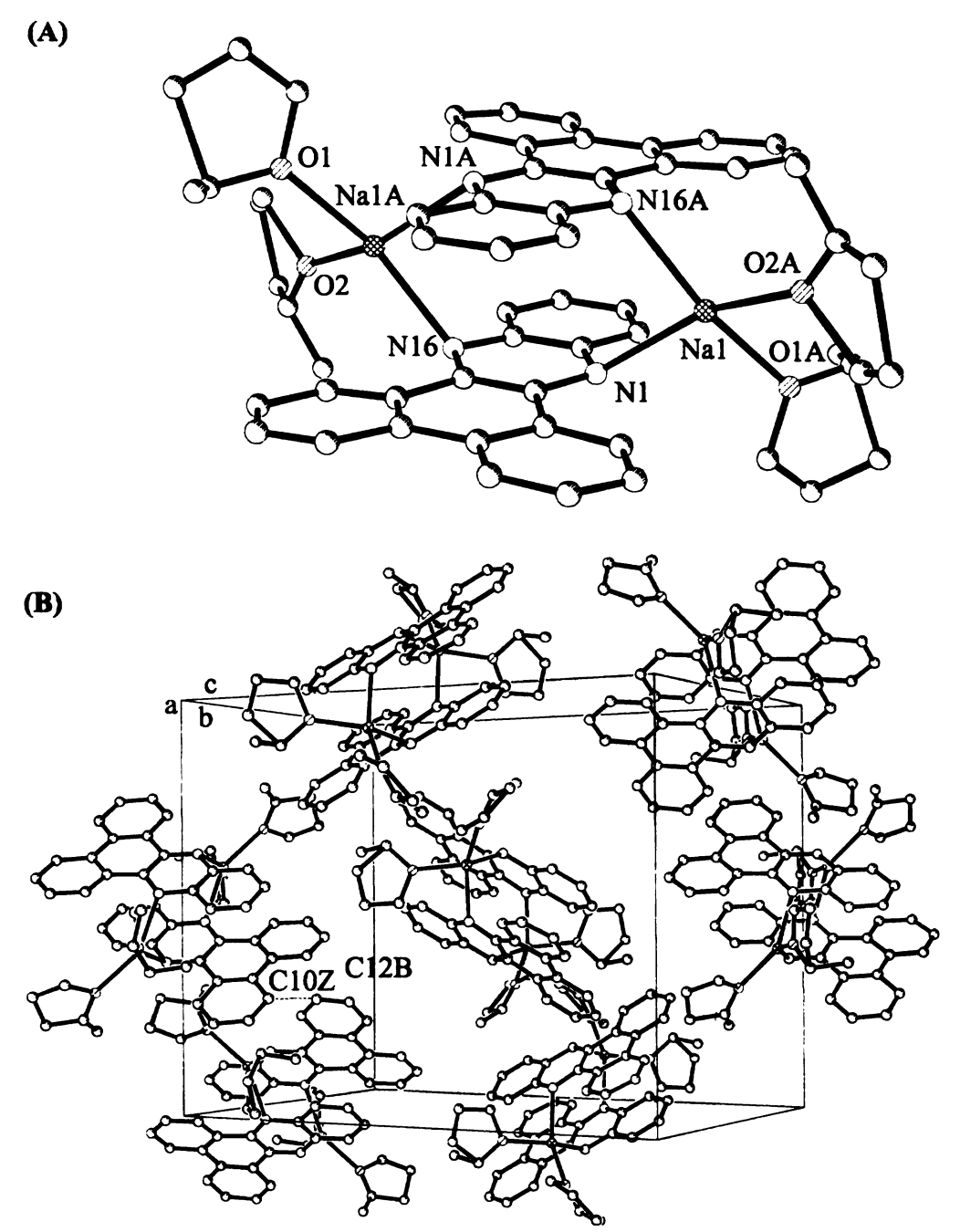


Figure 3.3 Single crystal X-ray structure of Na<sup>+</sup>(Dibenzo[a,c]phenazine) (MTHF)<sub>2</sub> with atom labeling using atomic symbols. (A) A single dimer is displayed. (B) Crystal packing for the unit cell with the shortest distance between dimers depicted by a dashed line. Only seven of twelve dimers in the unit cell are depicted in this Figure for clarity.

Comparisons will be made to the Na<sup>+</sup>(2,3-diphenylquinoxaline)<sup>-</sup> (DME) crystal structure reported by Bock and co-workers throughout this discussion.<sup>26</sup>

The two dibenzophenazine anions of the dimer displayed in Figure 3.1a, "pancake" onto one another and are connected through two  $N^{\delta}$ - $Na^{+}$ - $N^{\delta}$  bridges that are offset by 0.27 Å and -0.27 Å from the plane of the four nitrogen atoms. The dimer exhibits  $C_i$  symmetry inverting equivalent sets of atoms through a point in the center (i.e. N16 into N16A, C14 into C14A). The mean molecular planes of the  $\pi$  systems are parallel with stacking distances ranging from 3.245 Å at the nitrogens to 3.416 Å at C18. Two coordination sites of the sodium ion are occupied by MTHF oxygens, to complete a tetrahedral environment around the metal. It is interesting to note that the cations do not directly interact with the in-plane sp<sup>2</sup> lone pair of the quinoxaline nitrogens, but are offset by 42° from the plane of the quinoxaline moiety. This contrasts to the direct chelation of the sodium cation to the nitrogen nonbonding electrons of the 2,3-diphenylquinoxaline radical anion.

The metal appears not to interact significantly with the carbon framework. The shortest C-Na distance of 3.09 Å is considerably longer then those to the electron rich oxygen and nitrogens that average 2.33 Å and 2.43 Å respectively. In contrast, two sodium-carbon contacts of 3.06 Å were reported for the 2,3-diphenylquinoxaline salt to complete a pseudo-octahedral environment around the metal. Spatial arrangements and the rigidity of the dibenzo[a,c]phenazine framework apparently prevent such close metal-carbon contacts that would allowing sodium to attain its preferred coordination sphere of six. The dibenzo[a,c]phenazine skeleton is not precisely planar, but slightly curved at the

phenanthrene subunit, with atoms C5 and C12 being situated 0.19 Å and 0.18 Å from the mean molecular plane of the phenazine moiety.

**Table 3.2.** Selected Distances and Angles for Na<sup>+</sup>(Dibenzo[a,c]phenazine)<sup>-</sup> (2-MTHF)<sub>2</sub>. Distances are given in Å.

Distances			
Na(1)-O(2A)	2.315(4)	O(1A)-Na(1)-N(16A)	153.5(2)
Na(1)-O(1A)	2.344(3)	O(2A)-Na(1)-N(1)	151.5(2)
Na(1)-N(16A)	2.422(3)	O(1A)-Na(1)-N(1)	94.9(1)
Na(1)-N(1)	2.434(3)	N(16A)-Na(1)-N(1)	83.8(1)
Na(1)-C(4)	3.094(5)	O(2A)-Na(1)-C(4)	94.4(2)
	• •	O(1A)-Na(1)-C(4)	98.2(2)
Angles		N(16A)-Na(1)-C(4)	58.8(1)
O(2A)-Na(1)-O(1A)	88.4(2)	N(1)-Na(1)-C(4)	112.9(1)
O(2A)-Na(1)-N(16)	105.3(2)		, ,

The packing of the crystal showing a unit cell is displayed in Figure 3.3B. An inversion point lies on each edge of the unit cell with one residing in the center of the box. The smallest distance between dimers in the unit cell is 3.43Å as measured by the shortest (C-C) distance (shown as a dashed line in Figure 3.1b). All dimers in the cell are crystallographically equivalent.

The magnetic susceptibility of a powder sample was recorded for the Na<sup>+</sup>(dibenzo[a,c]phenazine)<sup>-</sup> (2-MTHF)<sub>2</sub> salt in the temperature range 2-300K. The solid line through the data points represent a least squares fit of the magnetic susceptibility data to the Bleaney-Bowers equation for magnetic coupling in isolated dimers.<sup>40</sup> The fit follows the curve at high temperatures with some deviation below 10K. A J/K of -22.2K indicates antiferromagnetic coupling between the two unpaired spins. The susceptibility reaches a maximum at 30°K of 0.136 emu/mol and falls precipitously to 0.0021 emu/mol

at 2K. The equation used to fit the data predicts a value of 3.6 \* 10<sup>-10</sup> emu/mol at 2.0K. It is not surprising to find some paramagnetism in the sample at low temperature.

The magnetic behavior appears to be consistent with the solid state structural data presented above. Long range order throughout the crystal lattice is precluded by the empty gaps between the dimers. The SOMO's between the two  $\pi$  systems should interact most strongly at the nitrogen, the site with the largest orbital coefficients and where the  $\pi$  systems come in closest proximity. Since the interaction is in-phase (or bonding) the nature of the coupling should be antiferromagnetic. It is uncertain to what extent exchange through sodium is operative, though it has been established through work done previously in this lab and others that the Na cation can act as a coupling unit. 9.17

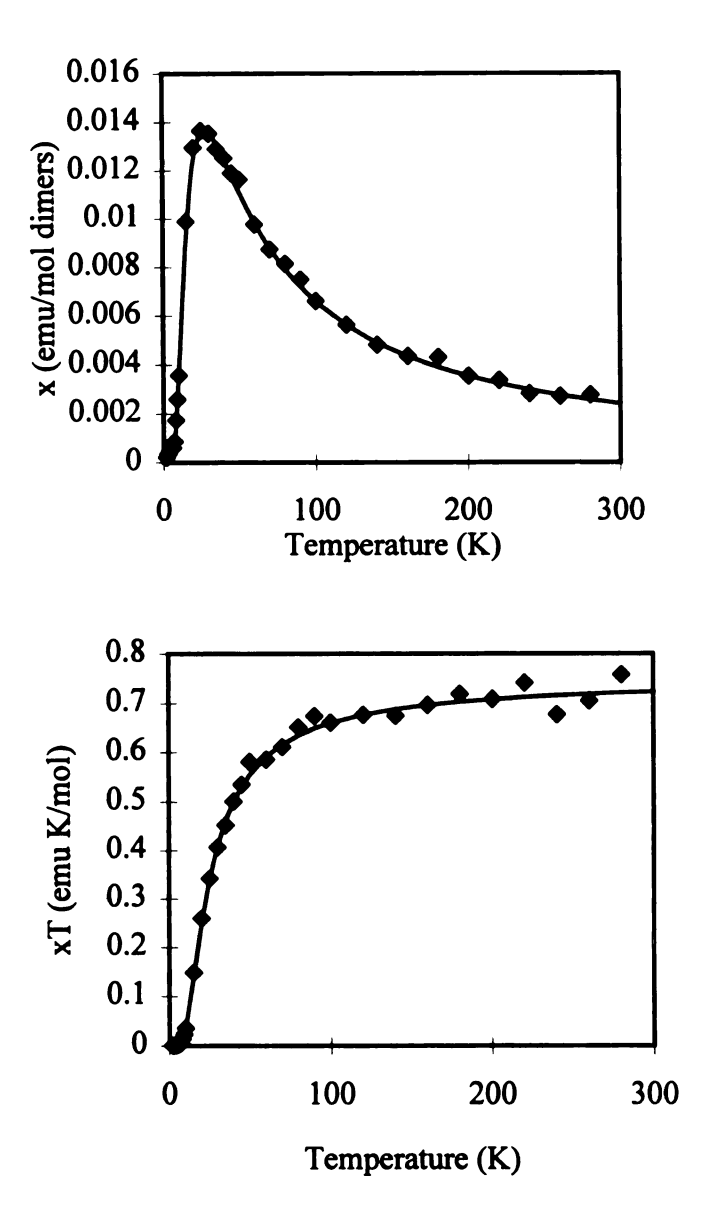


**Figure 3.4** Plot of molar susceptibility  $\chi$  vs temperature and  $\chi T$  vs temperature for a powder sample of the Na<sup>+</sup>(Dibenzo[a,c]phenazine)<sup>-</sup> (2-MTHF)<sub>1/3</sub> salt. The solid line represents a fit to the Bleaney-Bowers equation.

# 3.4 X-ray Structure and Magnetism of the K<sup>+</sup>(Dibenzo[a,c]phenazine)<sup>-</sup> (MTHF)<sub>2/3</sub> salt.

The K<sup>+</sup> (dibenzo[a,c]phenazine) (MTHF) salt crystallizes into the orthorhombic space group Pbca with six unique anions in the unit cell. Distances and angles are summarized in Table 3. In the crystal structure the radical anions are strung together by

N<sup>5</sup>-K<sup>+</sup>N<sup>5</sup> linkages to form the two crystallographically independent triple braided chains shown in Figure 3.5. The chains propagate along the c-axes by packing three unique dibenzophenazine anions into three separate stacks that are connected by potassium bridges to form a single "thick chain". The stacking distance is 5 Å with potassium cations residing between the stacks. Within the chain the dibenzo[a,c]phenazine anions are pointing in the same direction along the c-axis.

The coordination environments of the metals residing at the chain edge differ significantly from the one in the interior. The four metals on the edge interact with three nitrogens and one solvent oxygen with average K-N and K-O contact distances of 2.86 Å and 2.69 Å. The average K-N distances reported for the K<sup>+</sup>(2,3-Bis(2-Pyridyl) (THF)<sub>2</sub><sup>27</sup> and the K<sup>+</sup>(2,3-diphenylquinoxaline) (DME)<sup>26</sup> salt were respectively 2.9 Å and 2.8 Å. The coordination sphere of the metals are completed by contacts to three or four carbon atoms that are situated under 3.4 Å away. All K-C distances under 3.5 Å are displayed in Table 3.2. Two K-C contacts of 3.12 Å and 3.33 Å were reported for the diphenylquinoxaline salt.

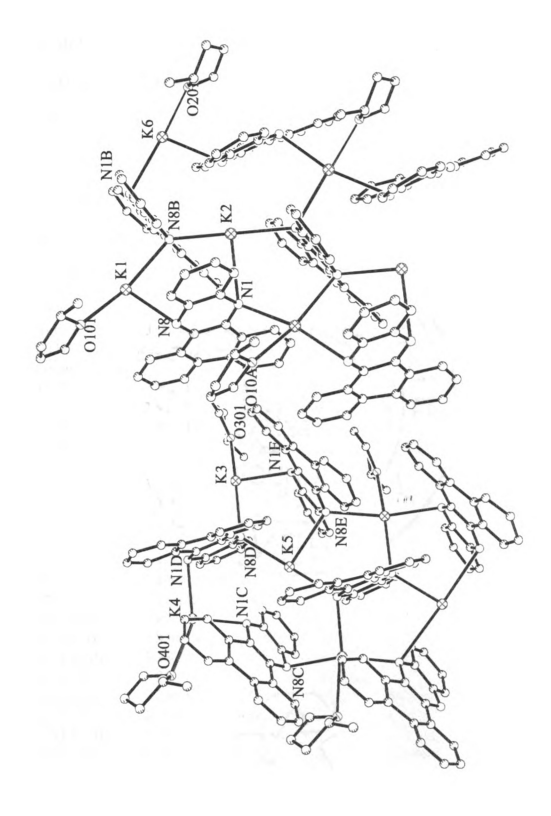


Table 3.3 Selected Distances and Angles for K'(Dibenzo[a,c]phenazine) (MTHF)23. Distances are given in Å

The environment of the cations residing in the center of the chains (K2 and K5) are free of solvent, with interactions only to three radical anions. The K2-N8A and K5-N1C distances are too long to complete a pseudo-square planer arrangement of nitrogens around the metal. Instead the metals interact with three nitrogens in a slightly distorted T geometry. All other nitrogen atoms in the crystal interact with two metals with K-N-K bond angles averaging 123°. For the K<sup>+</sup>(2,3-bis(2-pyridyl)(THF)<sub>2</sub> salt and the K<sup>+</sup>(2,3-diphenylquinoxaline) (DME) salts the potassium cation coordinated directly to the nitrogen lone pairs, but in the dimer based K<sup>+</sup>(2,3Bis(2-Pyridyl)(CH<sub>3</sub>NH<sub>2</sub>)<sub>3</sub> structure the K<sup>+</sup> is out of plane.

**Table 3.3** Selected Distances and Angles for K<sup>+</sup>(Dibenzo[a,c]phenazine). (MTHF)<sub>2/3</sub> Distances are given in Å.

Distances	unices are given		
K(1)-O(101)	2.72(2)	K(5)-C(2D)	3.45(2)
K(1)-O(101) K(1)-N(8)	2.810(14)	K(5)-C(2D) K(5)-C(3C)	3.26(2)
K(1)-N(1)	2.858(14)	K(6)-N(1A)	2.797(14)
K(1)-N(8B)	3.022(13)	K(6)-N(8A)	2.87(2)
K(1)-C(7B)	3.23(2)	K(6)-N(1B)	2.875(12)
K(1)-C(11)	3.31(2)	K(6)-O(201)	2.662(10)
K(1)-C(7)	3.39(2)	K(6)-C(2A)	3.30(2)
K(1)-C(20)	3.39(2)	K(6)-C(3A)	3.49(2)
K(1)-C(6B)	3.42(2)	K(6)-C(2B)	3.26(2)
K(1)-C(2)	3.44(2)	K(6)-C(11A)	3.24(2)
K(1)-C(3)	3.49(2)		
K(2)-N(1)	3.158(12)	Angles	
K(2)-N(8B)	2.81(2)	O(101)-K(1)-N(8)	94.3(4)
K(2)-N(1B)	2.850(14)	O(101)-K(1)-N(1)	80.0(4)
K(2)-C(20B)	3.24(2)	N(8)-K(1)-N(1)	166.9(4)
K(2)-C(3)	3.25(2)	O(101)-K(1)-N(8B)	164.6(5)
K(2)-C(6A)	3.26(2)	N(8)-K(1)-N(8B)	89.8(4)
K(2)-C(2)	3.25(2)	N(1)-K(1)-N(8B)	98.8(4)
K(2)-C(11B)	3.35(2)	K(1)-N(1)-K(2)	120.1(4)
K(2)-C(7A)	3.40(2)	K(2)-N(1B)-K(6)	124.8(5)
K(2)-C(7B)	3.40(2)	K(4)-N(1C)-K(5)	118.5(5)

Table 3.3 (Cont'd).

Table 3.5 (Cont	<del>u).</del>		
K(2)-C(2B)	3.44(2)	K(5)-N(1D)-K(4)	124.0(5)
K(6)-C(3B)	3.42(2)	N(8B)-K(2)-N(1B)	169.3(5)
K(6)-C(22B)	3.49(2)	N(8B)-K(2)-N(1)	94.8(4)
K(3)-O(301)	2.65(2)	N(1B)-K(2)-N(1)	87.9(4)
K(3)-N(8E)	2.877(14)	N(8B)-K(2)-C(20B)	115.9(5)
K(3)-N(8D)	2.904(13)	O(301)- $K(3)$ - $N(1E)$	92.1(4)
K(3)-N(1E)	2.806(14)	O(301)-K(3)-N(8E)	79.9(4)
K(3)-C(7D)	3.16(2)	N(1E)-K(3)-N(8E)	166.3(4)
K(3)-C(11E)	3.31(2)	O(301)-K(3)-N(8D)	164.5(5)
K(3)-C(6D)	3.36(2)	N(1E)-K(3)-N(8D)	91.8(4)
K(3)-C(20E)	3.37(2)	N(8E)-K(3)-N(8D)	98.9(4)
K(3)-C(7E)	3.45(2)	O(401)- $K(4)$ - $N(8C)$	94.3(5)
K(3)-C(22E)	3.49(2)	O(401)- $K(4)$ - $N(1D)$	149.0(6)
K(3)-C(2E)	3.41(2)	N(8C)-K(4)-N(1D)	96.8(4)
K(4)-N(1C)	2.89(2)	O(401)- $K(4)$ - $N(1C)$	80.4(5)
K(4)-N(8C)	2.77(2)	N(8C)-K(4)-N(1C)	159.9(5)
K(4)-N(1D)	2.886(13)	N(1D)-K(4)-N(1C)	97.6(4)
K(4)-O(401)	2.72(2)	N(8D)-K(5)-N(1D)	171.2(6)
K(4)-C(20C)	3.23(2)	N(8D)-K(5)-N(8E)	93.6(4)
K(4)-C(7C)	3.30(2)	N(1D)-K(5)-N(8E)	86.4(4)
K(4)-C(3D)	3.44(2)	N(8D)-K(5)-N(1C)	84.3(4)
K(4)-C(2D)	3.19(2)	N(1D)-K(5)-N(1C)	94.3(4)
K(5)-N(8D)	2.83(2)	N(8E)-K(5)-N(1C)	170.7(5)
K(5)-N(1D)	2.83(2)	O(201)- $K(6)$ - $N(1A)$	90.1(4)
K(5)-N(8E)	3.220(12)	O(201)- $K(6)$ - $N(8A)$	81.0(4)
K(5)-N(1C)	3.463(14)	N(1A)-K(6)-N(8A)	162.3(4)
K(5)-C(2C)	3.31(2)	O(201)- $K(6)$ - $N(1B)$	161.5(4)
K(5)-C(7E)	3.264(14)	N(1A)-K(6)-N(1B)	96.3(4)
K(5)-C(6E)	3.27(2)	N(8A)-K(6)-N(1B)	96.9(4)
K(5)-C(20D)	3.36(2)	K(2)-N(8B)-K(1)	124.6(5)
K(5)-C(7D)	3.39(2)	K(5)-N(8D)-K(3)	126.2(5)
K(5)-C(11D)	3.39(2)	K(3)-N(8E)-K(5)	120.0(4)

Magnetic susceptibility for the crystalline salt was recorded over the temperature range 2-300K. The  $\chi T$  vs T plot is displayed in Figure 3.6 along with a fit to the one dimensional Curie-Weiss model for magnetic coupling providing a Curie constant of 0.33emu/mol. The Weiss constant for the salt is found to be -12.6K indicating

antiferromagnetic behavior at low temperature. The weak magnetic interaction is a consequence of the large distance between the ligands and the inability of the K<sup>+</sup> to act as an efficient coupling unit. The K<sup>+</sup>(2,3-Bis(2-Pyridyl) (THF)<sub>2</sub> salt had a similar Weiss constant of -12°K. Although the one dimensional model appeared to fit the data well the chains do not represent a pure one dimensional system. Long range 3-D coupling is precluded by the nearly 5 Å distance between the chains.

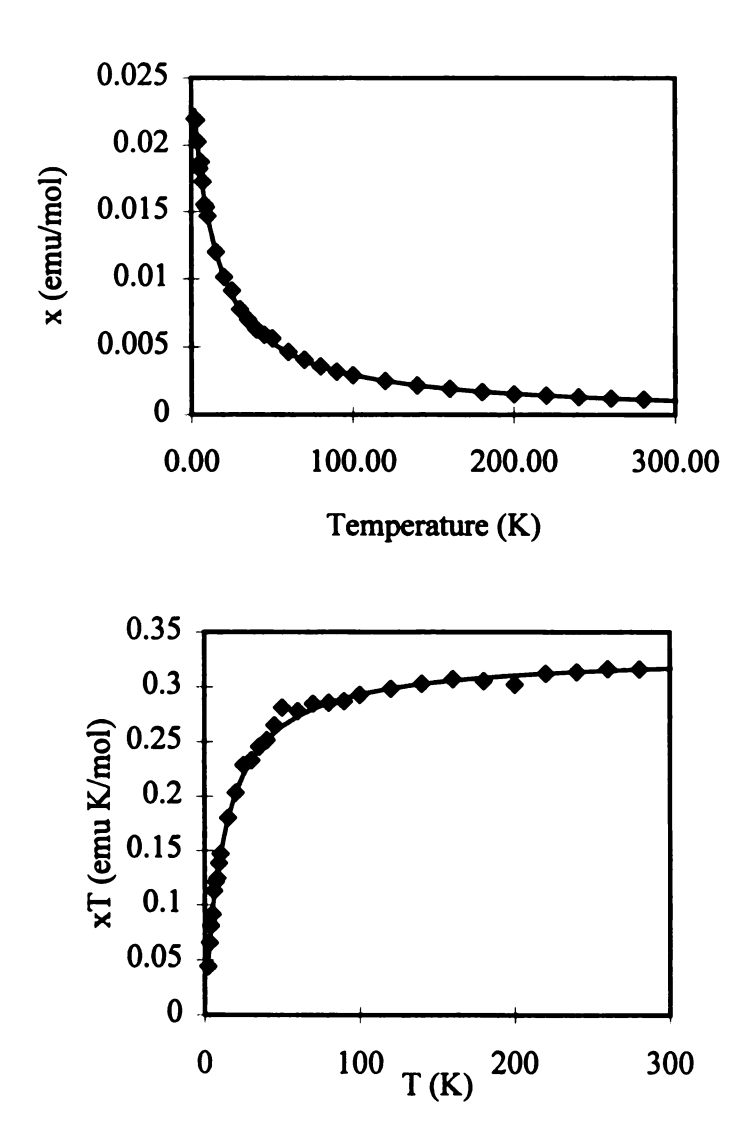


Figure 3.6 Plot of molar susceptibility  $\chi$  vs temperature and  $\chi$ t vs temperature for a powder sample of the K<sup>+</sup>(Dibenzo[a,c]phenazine) (2-MTHF)<sub>1/3</sub>salt. The solid line represents a fit to the Curie Weiss Equation for 1-D magnetic coupling.

The Rb<sup>+</sup> (dibenzo[a,c]phenazine) salt crystallizes in the orthorhombic space group Pbca with a single unique radical anion and metal cation in the unit cell. Dibenzo [a,c]phenazine radical anions linked through  $N^{\delta}$ -Rb<sup>+</sup>- $N^{\delta}$  bridges assemble into a solvent free 2-D network consisting of a  $N^{\delta}$ -Rb<sup>+</sup>- $N^{\delta}$ -(C-C)<sub>2</sub>- $N^{\delta}$ -Rb<sup>+</sup> pseudo-five membered ring

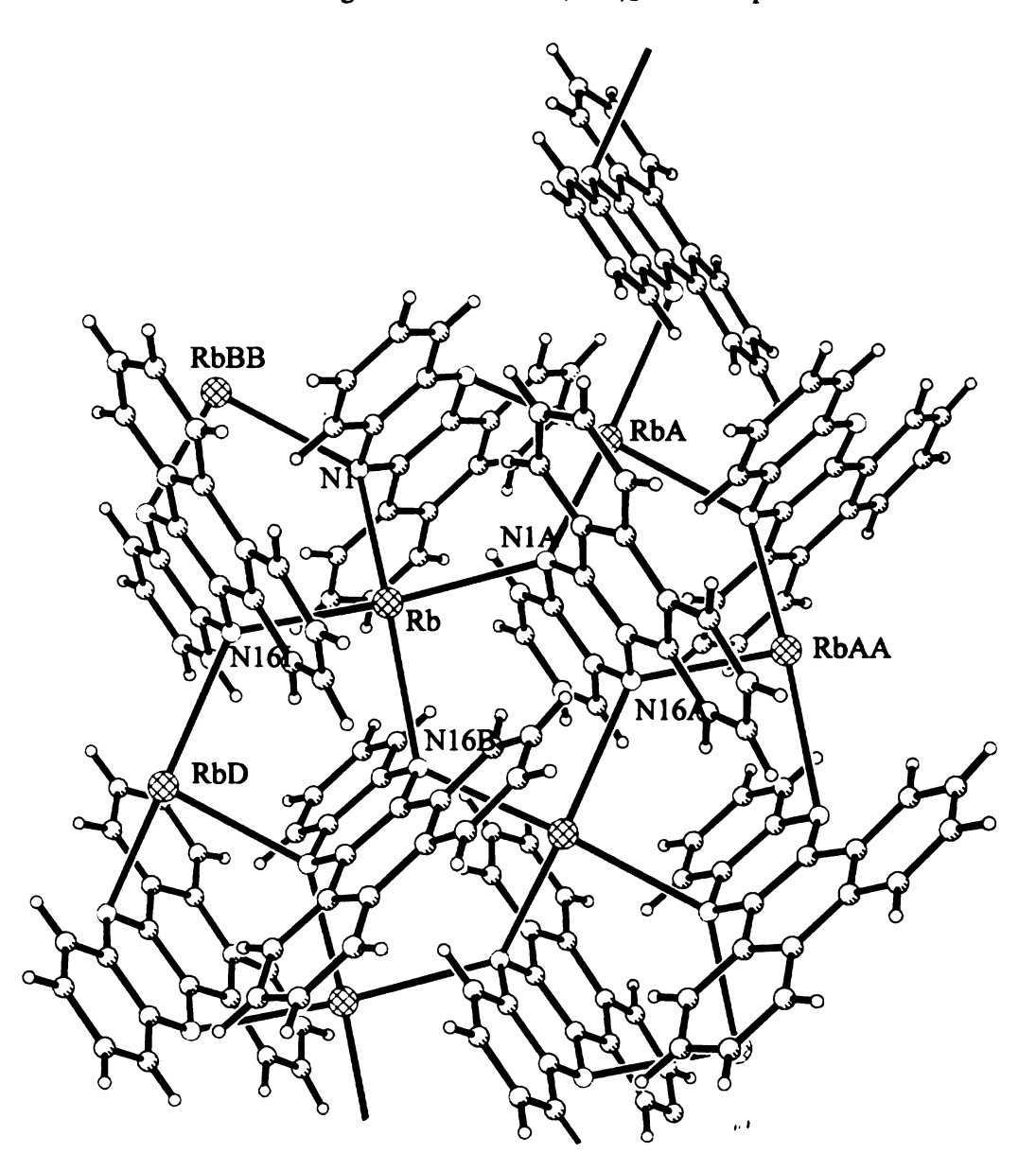


Figure 3.7 Single crystal X-ray structure of Rb<sup>+</sup> (Dibenzo[a,c]phenazine)- with atom labeling using atomic symbols.

connectivity pattern. The metals alternate by 0.28 Å above and below the least squares plane of the metals. The anions are alternately turned around the b-axis and are not packed in a parallel fashion.

The Rb<sup>+</sup> resides in a near square planer environment of four nitrogen atoms with an average Rb-N contact distance of 3.21 Å. This is greater then the average Rb-N distance of 3.07 Å I reported for the Rb<sup>+</sup>(2,3 bis-(3-methoxy-phenyl) quinoxaline)<sup>-</sup> (THF) salt. The longer Rb-N contacts may be attributed to the steric congestion arizing from packing four rigid dibenzo[a,c]phenazine ligands around the metal. The nearest carbon lies 3.36 Å away with four others within 3.5 Å, however the metal does not reside directly above the π system for optimal metal-carbon interactions.

The sheets are tightly packed together with the nearest distance between them being 2.45 Å as measured by the shortest (H-H) distance. Their packing leads to infinite cylindrical cavities approximately 2 Å between the sheets.

**Table 3.4.** Selected Distances and Angles for Rb<sup>+</sup>(Dibenzo[a,c]phenazine)<sup>-</sup> Distances are given in Å.

Λ.		
3.110(2)	N(16B)-Rb(1)-C(18B)	41.97(6)
3.150(2)	N(1)-Rb(1)-C(21A)	79.39(6)
3.256(2)	N(16I)-Rb(1)-C(21A)	145.18(6)
3.320(2)	N(1A)-Rb(1)-C(21A)	42.28(6)
3.360(2)	N(1)-Rb(1)-C(22)	22.73(5)
3.402(3)	N(16I)-Rb(1)-C(22)	96.38(6)
3.405(3)	N(1A)-Rb(1)-C(22)	80.37(5)
3.425(2)	N(16B)-Rb(1)-C(22)	174.01(5)
3.482(2)	N(16B)-Rb(1)-C(21A)	89.77(6)
3.524(2)	N(1)-Rb(1)-C(22A)	95.04(6)
3.553(2)	N(16I)-Rb(1)-C(22A)	164.03(5)
3.562(2)	N(1A)-Rb(1)-C(22A)	23.72(5)
	N(16B)-Rb(1)-C(22A)	80.73(6)
	N(1)-Rb(1)-C(17B)	138.50(5)
89.92(5)	N(16I)-Rb(1)-C(17B)	77.84(5)
89.69(4)	N(1A)-Rb(1)-C(17B)	107.48(5)
172.06(5)	N(16B)-Rb(1)-C(17B)	22.74(5)
159.78(5)	N(1)-Rb(1)-C(15I)	84.37(5)
89.39(4)	N(16I)-Rb(1)-C(15I)	23.21(5)
93.70(5)	N(1A)-Rb(1)-C(15I)	148.97(5)
123.26(6)	N(16B)-Rb(1)-C(15I)	102.30(5)
50.89(6)	N(1)-Rb(1)-C(14I)	99.66(5)
70.56(5)	N(16I)-Rb(1)-C(14I)	42.05(5)
117.84(6)	N(1A)-Rb(1)-C(14I)	130.33(5)
85.71(6)	N(16B)-Rb(1)-C(14I)	93.30(5)
101.46(6)	Rb(1)-N(1)-Rb(BB)	125.16(6)
	3.110(2) 3.150(2) 3.256(2) 3.320(2) 3.360(2) 3.402(3) 3.405(3) 3.425(2) 3.524(2) 3.553(2) 3.562(2) 89.92(5) 89.69(4) 172.06(5) 159.78(5) 89.39(4) 93.70(5) 123.26(6) 50.89(6) 70.56(5) 117.84(6) 85.71(6)	3.110(2) N(16B)-Rb(1)-C(18B) 3.150(2) N(1)-Rb(1)-C(21A) 3.256(2) N(16I)-Rb(1)-C(21A) 3.320(2) N(1A)-Rb(1)-C(21A) 3.360(2) N(1)-Rb(1)-C(22) 3.402(3) N(16I)-Rb(1)-C(22) 3.405(3) N(1A)-Rb(1)-C(22) 3.425(2) N(16B)-Rb(1)-C(22) 3.482(2) N(16B)-Rb(1)-C(21A) 3.524(2) N(16B)-Rb(1)-C(22A) 3.553(2) N(16I)-Rb(1)-C(22A) N(16B)-Rb(1)-C(22A) N(16B)-Rb(1)-C(22A) N(16B)-Rb(1)-C(17B) 89.92(5) N(16I)-Rb(1)-C(17B) 172.06(5) N(16B)-Rb(1)-C(17B) 172.06(5) N(16B)-Rb(1)-C(17B) 159.78(5) N(1)-Rb(1)-C(15I) 159.78(5) N(16I)-Rb(1)-C(15I) 123.26(6) N(16B)-Rb(1)-C(15I) 123.26(6) N(16B)-Rb(1)-C(15I) 123.26(6) N(16B)-Rb(1)-C(14I) 17.84(6) N(1A)-Rb(1)-C(14I) 117.84(6) N(1A)-Rb(1)-C(14I) 85.71(6) N(16B)-Rb(1)-C(14I)

## 3.5. Summary

The Na<sup>+</sup>(Dibenzo[a,c]phenazine) (MTHF)<sub>2</sub>, K<sup>+</sup>(Dibezo[a,c]phenazine) (2-MTHF)<sub>2/3</sub>, Rb<sup>+</sup>(Dibenzo[a,c]phenazine) salts exhibit remarkable structural differences based on variations in the ionic radii of the metal. Many questions surrounding the topic of how and why molecules assemble into a given crystal lattice remain unanswered. The size of the alkali metal and its ability to coordinate to solvent no doubt plays an important

role in dictating the dimensionality of these structures. The sodium cation interacts with only two radical anions forming simple dimers with the remaining two coordination sites effectively "solvated." In stark contrast the large solvent free rubidium cation can interact with four radical anions to result in a two dimensional network.

Crystallizing in a weakly chelating and sterically demanding solvent such as MTHF may lead to higher dimensional systems then solvents such as gylme and diglyme that tend to more effectively compete for the coordination sphere of the metal. The potassium cation in the K<sup>+</sup>(diphenyquinoxaline)<sup>-</sup>(DME) salt was chelated to two dimethoxyethane oxygens and two radical anions to form a one dimensional chain. In contrast the metal in the K<sup>+</sup>(dibenzo[a,c]phenazine)<sup>-</sup>(MTHF)<sub>2/3</sub> salt could only interact with three radical anions.

It is not completely certain to what extent the carbon framework participates in the coordination environment of the metals. The metals do not reside directly above the carbon framework to interact strongly with the  $\pi$  system as do the alkali metal salts of the perylene radical anion. In that particular case C-Na contacts under 2.9 Å were reported. The strongest electrostatic interaction will occur on the nitrogen where most of the negative charge is localized. In all the crystal structures I reported each nitrogen is chelated directly to two alkali metal cations with M<sup>+</sup>-N-M<sup>+</sup> bond angles near 120°. The crystal structure for the diphenylquinoxaline salts had the metals in the sp<sup>2</sup>N plane.

The structural motif of these systems provided only for antiferromagnetic interactions. In the rubidium and potassium salts the paramagnetic centers were to far apart to attain significant orbital overlap, giving rise to small Curie constants. However

the sodium salt possessed comparatively strong magnetic coupling due to the shorter distance between the radical centers. Unfortunately, the greater solvation of the sodium cation limited the dimensionality of the system to isolated dimers. This appears to underscore the challenge of reducing cation solvation in the crystal lattice and at the same time providing for short distances between radical anions.

## Chapter 4

## Experimental

4.1	Ligand Synthesis and Purification	49
4.2	Solvent Purification	49
4.3	Synthesis of the Radical Anion Salts	.50
4.4	Crystallization of the Radical Anion Salts	50
4.5	X-ray analysis	.51
4.6	EPR and ENDOR Analysis	.52
4.7	Magnetic Susceptibility Analysis	.52

### 4.1 Ligand Synthesis and Purification

Dibenzo[a,c]phenazine was synthesized by adding an acetic acid solution of phenanthroquinone to a refluxing acetic acid solution of o-phenylenediamine. The product precipitated almost immediately following the addition. The solid was filtered and purified by recrystallizing three times in CH<sub>2</sub>Cl<sub>2</sub>/CHCl<sub>3</sub>. The bis-2-methoxyphenyl quinoxaline was already prepared and purified by Lawrence P. Szajek.

#### 4.2 Solvent Purification

Reagent grade tetrahydrofuran (300ml) was pre-dried by refluxing over NaK in the presence of benzophenone for about 24 hours. About two thirds of the blue solution was distilled and placed into a 300ml bottle fitted with a Teflon stopcock. The bottle was placed on the vacuum line (10<sup>-5</sup> torr) and three freeze-pump-thaw cycles were carried out before distilling the solution over NaK. More freeze-pump-thaw cycles were done until the solution turned an aqua blue.

Anhydrous 2-Methyltetrahydrofuran (200ml) was poured into a bottle fitted with a Teflon stopcock under a nitrogen atmosphere. The solution underwent multiple freeze-pump-thaw cycles at 10<sup>-5</sup> torr until the bubbling stopped. It was then distilled over NaK where a final freeze-pump-thaw cycle was carried out.

Pentane (300ml) was pre-dried by boiling over Na for about six hours. The solution was distilled and placed in a 300mL bottle where it was freeze-pump-thawed three times on a high vacuum line(10<sup>-5</sup>) torr. The solvent was distilled over NaK.

### 4.3 Synthesis of the Radical Anion Salts

M\*(Dibenzo[a,c]phenazine) (M = Na, K, Rb): Dibenzo[a,c]phenazine (40mg, 0.143mmol) was introduced into chamber 1 of the H-cell shown below, fitted with 3mm EPR quartz tubes or an optical cell with a 1mm path length in place of one of the tubes. In a helium dry box a slight excess of alkali metal was added to chamber two. The cell was then attached to a vacuum line at 10<sup>-5</sup> torr where the alkali metal was sublimed into a shiny metal mirror by heating with a torch. Chamber 1 was submerged into liquid nitrogen, into which dry THF (30ml) was distilled. The cell was warmed to dissolve the ligand and then cooled down in a dry ice/isopropanol bath to -60°C. The THF solution was added to the sodium metal mirror resulting in a red reaction mixture of the radical anion salt. Most of the mirror was consumed.

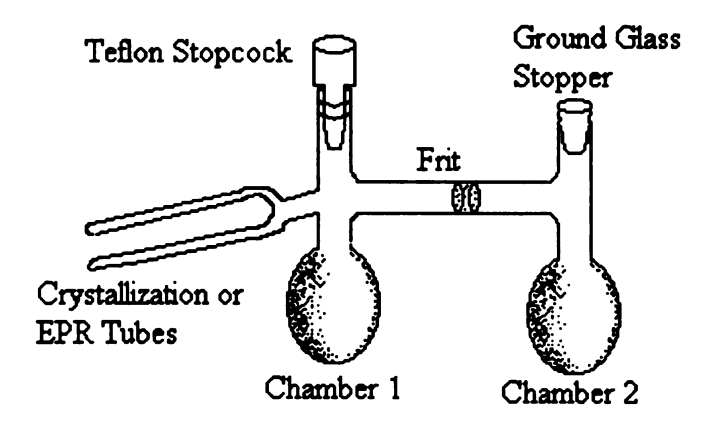


Figure 4.1 A modified H cell.

### 4.4 Crystallization of the Radical Anion Salts.

M<sup>+</sup>(Dibenzo[a,c]phenazine) (M = Na, K, Rb) The modified H cell in Figure 4.1 was fitted with two 18mm Pyrex tubes. Synthesis of the radical anion salt was carried out in 30 ml of MTHF using the same procedure discussed above with 100mg of

dibenzo[a,c]phenazine and a small excess of metal. The red MTHF solution was poured into the crystallization tube and about one quarter of the solvent removed through evaporation. The solution was submerged in liquid nitrogen and about an equal volume of pentane was distilled in. The Pyrex tube was sealed off with a torch. The solution was allowed to thaw slowly by first completely thawing the pentane layer then the MTHF layer. This was done to minimize the disturbance around the solvent interface. The two solvents were allowed to diffuse for 2-3 weeks with black lustrous needles forming for the sodium and potassium salts. Black blocks were formed of the rubidium salt.

Rb<sup>+</sup>(2,3 bis-(3-methoxyphenyl) quinoxaline)<sup>-</sup> The exact same procedure as above was used except 150 mg of 2,3 bis-(3-methoxyphenyl) quinoxaline was dissolved in 30ml of THF. About ¼ of the solvent was evaporated before being capped with pentane. The solvents were allowed to diffuse together for 1 week. Lustrous dark blue needles resulted.

#### 4.5 X-ray analysis.

The crystallization tubes were opened up in a nitrogen glove box and the solvent was decanted off. The crystals were washed out with octane and poured onto a copper block at about -30°C. A single crystal was removed from the octane and coated with viscous oil. It was then mounted on a glass fiber. The crystal structures were solved by Rui Huang using direct methods (SHELXS-93) and refined by full matrix least-squares procedures using TEXSAN. All atoms were refined anisotropically. The hydrogen atoms were not refined, except for the Rb<sup>+</sup>(Dibenz[a,c]phenazine)<sup>-</sup> structure.

### 4.6 EPR and ENDOR Analysis.

EPR and ENDOR spectra were recorded on a Bruker ESP300E spectrometer.

Typical parameters were: modulation frequency of 12.5kHz, Modulation amplitude

0.290gauss, Power = 2.51 mW, and receiver gain = 100000. All samples were prepared in THF at a concentration near 0.001moler

### 4.7 Magnetic Susceptibility Analysis.

The temperature dependence on the magnetic susceptibility for the crushed polycrystalline samples were determined with a Quantum Design MPMS2 SQUID magnetometer. Crystals of the radical anions were placed inside a plastic bag in a helium dry box (>1ppm of oxygen). The temperature dependence of the susceptibility was measured over the temperature range 2-300K. The susceptibility of the plastic bag was measured separately and its diamagnetism was subtracted from the signal. Pascal's constants were used to account for the diamagnetism within the sample.

Appendix

X-ray Data

Table A2.7 Single crystal X-ray refinement data.

	Rb <sup>+</sup> (Methquinox) (THF)	Na <sup>+</sup> (Dibphz) (2-MTHF) <sub>2</sub>	Rb <sup>+</sup> (Methquinox) (THF) Na <sup>+</sup> (Dibphz) (2-MTHF) <sub>2</sub> K <sup>+</sup> (Dibphz) (2-MTHF) <sub>23</sub> Rb <sup>+</sup> (Dibphz)	Rb <sup>+</sup> (Dibphz)
Molecular Formula	C22H12O2N2Rb+C4HgO	$C_{20}H_{12}N_2Na^++(C_5H_9O)_2$ $C_{120}H_{72}N_{12}K_6+(C_5H_9O)_4$	C120H72N12K6+ (C5H9O)4	C <sub>20</sub> H <sub>12</sub> N <sub>2</sub> Rb
Formula Weight	463.5	473	2254.6	365.47
Temperature(°K)	173	173	173	173
Crystal System	Orthorhombic	Orthorhombic	Orthorhombic	Orthorhombic
Space Group	Pbca	Pbca	Pbca	Pbca
a, Å	8.068(2)	16.668(3)	7.6740(3)	8.068(2)
b, A	21.830(4)	14.786(3)	31.3734(8)	21.830(4)
c, A	26.340(5)	20.895(4)	44.489(2)	26.347(5)
Volume, A <sup>3</sup>		5149(2)	10711.1(7)	3025.7(11)
Density g/cm <sup>3</sup>	1.3	1.3	0.942	1.8
Reflections Collected	49305	28803	24785	17387
us	5648	6178	12114	3657
wR1	0.0447	0.0917	0.119	0.0404
wR2	0.0775	0.3806	0.2591	0.0968

**Table 2A** Atomic Coordinates and Isotropic Displacement Parameters for Rb<sup>+</sup> (2,3 bis-(3-methoxyphenyl) quinoxaline) (THF).

	х	у	Z	U(eq)
Rb	1662(1)	218(1)	1856(1)	32(1)
N(1)	5318(2)	199(1)	1996(1)	21(1)
C(2)	5922(3)	-393(1)	1963(1)	20(1)
C(3)	5129(3)	-870(1)	2226(1)	25(1)
C(4)	5657(3)	-1476(1)	2176(1)	29(1)
C(5)	6994(3)	-1615(1)	1865(1)	27(1)
C(6)	7828(3)	-1149(1)	1608(1)	23(1)
C(7)	7343(3)	-533(1)	1658(1)	19(1)
N(8)	8255(2)	-76(1)	1426(1)	20(1)
C(9)	7637(3)	504(1)	1466(1)	18(1)
C(10)	8746(3)	981(1)	1242(1)	19(1)
C(11)	9616(3)	851(1)	789(1)	21(1)
C(12)	10715(3)	1281(1)	587(1)	23(1)
O(13)	11602(2)	1198(1)	147(1)	32(1)
C(14)	11196(3)	682(1)	-164(1)	34(1)
C(15)	10982(3)	1835(1)	832(1)	28(1)
C(16)	10153(3)	1961(1)	1281(1)	27(1)
C(18)	9051(3)	1539(1)	1483(1)	24(1)
C(19)	6150(3)	634(1)	1720(1)	19(1)
C(20)	5329(3)	1248(1)	1719(1)	20(1)
C(21)	4482(3)	1451(1)	2151(1)	26(1)
C(22)	3778(3)	2034(1)	2161(1)	31(1)
C(23)	3917(3)	2422(1)	1750(1)	28(1)
C(24)	4705(3)	2216(1)	1314(1)	24(1)
O(25)	4744(2)	2627(1)	917(1)	35(1)
C(26)	5592(5)	2440(2)	468(1)	63(1)
C(27)	5371(3)	1631(1)	1290(1)	22(1)
O(101)	2781(2)	-430(1)	966(1)	43(1)
C(102)	4182(3)	-328(1)	647(1)	37(1)
C(103)	4148(4)	-850(2)	271(1)	47(1)
C(104)	3497(5)	-1375(2)	586(2)	74(1)
C(105)	2638(4)	-1080(1)	1031(1)	50(1)

**Table 3A** Atomic Coordinates and Isotropic Displacement Parameters for Na<sup>+</sup>(Dibenzo[a,c]phenazine)<sup>-</sup> (MTHF)<sub>2</sub>.

	x	y , , , , , , , , , , , , , , , , , , ,	Z	U(eq)
Na(1)	1019(1)	3138(1)	30(1)	49(1)
N(1)	-345(2)	3674(2)	-139(1)	38(1)
C(2)	-805(2)	3975(2)	355(1)	36(1)
C(3)	-806(2)	3470(2)	955(2)	42(1)
C(4)	-381(2)	2640(3)	1000(2)	53(1)
C(5)	-344(3)	2179(3)	1578(2)	70(1)
C(6)	-717(3)	2528(4)	2118(2)	78(2)
C(7)	-1152(3)	3305(4)	2068(2)	68(1)
C(8)	-1215(2)	3804(3)	1493(2)	51(1)
C(9)	-1696(2)	4610(3)	1440(2)	56(1)
C(10)	-2143(3)	4974(4)	1961(2)	79(2)
C(11)	-2630(4)	5714(5)	1876(4)	110(3)
C(12)	2701(4)	3859(4)	-1294(4)	103(2)
C(13)	2275(3)	4182(3)	-772(3)	76(1)
C(14)	1750(2)	4936(2)	-850(2)	50(1)
C(15)	1274(2)	5232(2)	-306(2)	39(1)
N(16)	1300(2)	4719(2)	233(1)	44(1)
C(17)	-881(2)	4941(2)	-749(2)	42(1)
C(18)	-912(3)	5400(3)	-1346(2)	63(1)
C(19)	-495(3)	5096(4)	-1864(2)	73(1)
C(20)	-22(3)	4318(4)	-1817(2)	69(1)
C(21)	24(2)	3858(3)	-1243(2)	55(1)
C(22)	-408(2)	4155(2)	-701(1)	40(1)
O(101)	886(3)	1868(2)	-633(2)	89(1)
O(201)	1967(3)	2347(3)	616(2)	118(2)
C(103)	1327(6)	1818(7)	-1735(4)	141(4)
C(104)	119(11)	906(10)	-1291(8)	284(12)
C(106)	841(10)	510(10)	-1251(7)	202(6)
C(105)	96(6)	1496(5)	-768(4)	126(3)
C(202)	1773(7)	1221(7)	682(7)	160(4)
C(102)	1451(8)	1523(8)	-1070(6)	170(5)
C(203)	2047(8)	938(8)	1269(9)	191(6)
C(205)	2543(12)	2240(31)	929(13)	484(27)
C(204)	2739(5)	1834(8)	1483(4)	138(4)
C(206)	2907(8)	3229(9)	1005(12)	251(11)

**Table 4A** Atomic Coordinates and Isotropic Displacement Parameters for K<sup>+</sup>(Dibenzo[a,c]phenazine) (MTHF)<sub>2/3</sub>.

	X	у	Z	U(eq)
K(1)	9623(5)	2903(1)	116(1)	34(1)
N(1)	3227(18)	3070(4)	226(4)	21(4)
N(1A)	3368(18)	5524(4)	138(4)	21(4)
N(1B)	11154(18)	4300(4)	242(4)	16(3)
N(1C)	1337(20)	-984(4)	2920(4)	27(4)
N(1D)	6117(20)	-241(4)	2939(4)	29(4)
N(1E)	1105(18)	1492(4)	3042(4)	25(4)
K(2)	4665(5)	4011(1)	194(1)	36(2)
C(2)	3940(26)	3058(5)	-65(5)	29(5)
C(2A)	4112(26)	5285(5)	-71(5)	28(5)
C(2B)	10397(25)	4156(5)	-22(4)	17(5)
C(2C)	529(27)	-954(5)	3185(6)	35(6)
C(2D)	5341(26)	-112(5)	3186(5)	30(5)
C(2E)	311(24)	1272(5)	3267(5)	20(5)
K(3)	4482(5)	1151(1)	3015(1)	34(1)
C(3)	3176(24)	3313(5)	-280(5)	23(5)
C(3A)	3469(26)	5280(5)	-358(5)	27(5)
C(3B)	10956(27)	4311(5)	-303(5)	32(5)
C(3C)	1150(28)	-688(6)	3430(6)	39(6)
C(3D)	5997(25)	-222(5)	3468(5)	29(5)
C(3E)	860(24)	1282(5)	3561(5)	21(5)
K(4)	5002(5)	-1107(1)	3044(1)	31(1)
C(4)	3899(27)	3296(6)	-578(5)	35(6)
C(4A)	4136(28)	5038(5)	-614(5)	28(5)
C(4B)	10239(27)	4154(6)	-577(5)	32(5)
C(4C)	477(27)	-692(5)	3714(5)	35(5)
C(4D)	5337(27)	-63(6)	3739(5)	35(5)
C(4E)	190(25)	1044(5)	3789(5)	24(5)
K(5)	-372(6)	34(1)	2975(1)	42(2)
C(5)	5249(24)	3032(5)	-653(4)	23(5)
C(5A)	5502(28)	4768(6)	-528(5)	35(6)
C(5B)	8844(28)	3877(6)	-563(5)	36(5)
C(5C)	-1012(31)	-957(6)	3787(5)	43(6)
C(5D)	3898(27)	207(6)	3734(5)	29(5)
C(5E)	-1231(24)	759(5)	3719(5)	24(5)
K(6)	10035(5)	5164(1)	149(1)	36(1)
C(6)	6023(26)	2781(5)	-421(5)	29(5)
C(6A)	6203(26)	4753(5)	-244(5)	31(5)
C(6B)	8122(25)	3751(5)	-291(5)	28(5)
C(6C)	-1581(28)	-1225(6)	3561(5)	34(6)
C(6D)	3198(26)	332(5)	3447(5)	24(5)

Table 4A (Cont'd).

1 able 4A (C	zoni a).			
C(6E)	-1934(29)	753(6)	3434(5)	37(6)
C(7)	5474(24)	2797(5)	-135(5)	21(5)
C(7A)	5590(26)	5026(5)	-19(5)	24(5)
C(7B)	8922(26)	3903(5)	-6(5)	25(5)
C(7C)	-924(27)	-1226(6)	3264(5)	28(5)
C(7D)	3838(22)	186(5)	3183(4)	15(4)
C(7E)	-1173(21)	1011(4)	3186(4)	9(4)
N(8)	6216(18)	2576(4)	92(4)	20(4)
N(8A)	6406(21)	5026(4)	268(4)	30(4)
N(8B)	8180(20)	3775(4)	260(4)	27(4)
N(8C)	-1712(20)	-1472(4)	3040(4)	32(4)
N(8D)	3143(19)	298(4)	2914(4)	22(4)
N(8E)	-1880(17)	988(4)	2910(3)	17(3)
C(9)	5508(24)	2571(5)	367(4)	19(4)
C(9A)	5776(24)	5303(5)	465(4)	18(4)
C(9B)	8922(25)	3904(5)	507(5)	21(4)
C(9C)	-888(25)	-1477(5)	2784(5)	30(5)
C(9D)	3899(23)	139(5)	2645(4)	15(4)
C(9E)	-1139(26)	1244(5)	2707(5)	29(5)
C(10)	6343(25)	2337(5)	606(5)	26(5)
C(10A)	6617(28)	5365(6)	737(5)	36(6)
C(10B)	8208(24)	3807(5)	800(5)	15(4)
C(10C)	-1579(26)	-1759(5)	2554(5)	27(5)
C(10D)	3109(24)	237(5)	2364(5)	20(5)
C(10E)	-1931(24)	1265(5)	2408(5)	17(4)
C(11)	7959(27)	2128(5)	532(5)	30(5)
C(11A)	8213(27)	5137(5)	805(5)	29(5)
C(11B)	6573(25)	3590(5)	803(5)	27(5)
C(11C)	-3209(28)	-1968(6)	2604(6)	38(6)
C(11D)	1540(22)	455(5)	2355(4)	12(4)
C(11E)	-3501(27)	1043(5)	2361(5)	38(5)
C(12)	8739(27)	1906(5)	769(S)	34(5)
C(12A)	9188(25)	5223(5)	1053(4)	23(5)
C(12B)	5777(24)	3499(5)	1083(5)	21(5)
C(12C)	-3899(29)	-2211(6)	2366(6)	32(6)
C(12D)	731(22)	523(4)	2091(4)	14(4)
C(12E)	-4352(26)	1101(5)	2087(5)	31(5)
C(13)	8107(26)	1905(5)	1061(5)	29(5)
C(13A)	8633(25)	5546(5)	1259(5)	26(5)
C(13B)	6538(26)	3663(5)	1343(5)	31(5)
C(13C)	-3088(29)	-2260(6)	2100(5)	37(6)
C(13D)	1460(28)	379(6)	1811(5)	36(5)
C(13E)	-3641(27)	1363(6)	1844(5)	38(5)
	( )	(-)	-3(8)	(-)

Table 4A (Cont'd).

Table 4A (C	one aj.			
C(14)	6545(26)	2115(5)	1120(5)	25(5)
C(14A)	7045(28)	5728(5)	1234(5)	35(6)
C(14B)	8132(24)	3852(5)	1339(4)	20(4)
C(14C)	-1532(27)	-2061(5)	2045(5)	26(5)
C(14D)	3077(26)	157(5)	1818(5)	26(5)
C(14E)	-1981(27)	1562(5)	1917(5)	29(6)
C(15)	5680(23)	2340(5)	903(4)	18(4)
C(15A)	6050(24)	5647(5)	971(4)	21(5)
C(15B)	8998(26)	3948(5)	1062(5)	18(5)
C(15C)	-748(25)	-1810(5)	2271(5)	24(5)
C(15D)	3869(25)	99(5)	2101(5)	23(5)
C(15E)	-1200(28)	1527(6)	2194(5)	35(6)
C(16)	3894(23)	2521(5)	962(4)	18(4)
C(16A)	4359(23)	5851(5)	918(4)	22(4)
C(16B)	10698(25)	4158(5)	1059(5)	27(5)
C(16C)	1031(26)	-1614(5)	2223(5)	27(5)
C(16D)	5598(22)	-118(4)	2112(4)	10(4)
C(16E)	554(26)	1738(5)	2259(5)	26(5)
C(17)	3169(25)	2492(5)	1237(5)	27(5)
C(17A)	3603(25)	6108(5)	1149(5)	29(5)
C(17B)	11612(26)	4244(5)	1304(5)	27(5)
C(17C)	1945(24)	-1689(5)	1967(4)	22(5)
C(17D)	6427(24)	-220(5)	1850(4)	20(5)
C(17E)	1433(27)	1941(5)	2003(5)	34(5)
C(18)	1494(27)	2675(5)	1288(5)	36(5)
C(18A)	1976(25)	6310(5)	1097(5)	29(5)
C(18B)	13127(28)	4450(5)	1309(5)	32(6)
C(18C)	3635(27)	-1486(6)	1924(5)	39(6)
C(18D)	8075(24)	-438(5)	1868(4)	21(4)
C(18E)	3083(28)	2142(5)	2078(5)	34(5)
C(19)	797(25)	2938(5)	1068(5)	23(5)
C(19A)	1173(24)	6274(5)	812(5)	22(5)
C(19B)	13823(26)	4598(5)	1039(5)	26(5)
C(19C)	4194(30)	-1179(6)	2129(5)	42(6)
C(19D)	8705(27)	-576(6)	2148(5)	37(5)
C(19E)	3749(31)	2134(6)	2371(6)	44(6)
C(20)	1593(23)	3004(5)	795(5)	21(4)
C(20A)	1897(24)	6007(5)	581(5)	22(5)
C(20B)	12959(25)	4522(5)	756(5)	29(5)
C(20C)	3196(25)			` '
C(20D)	7800(24)			• •
C(20E)	• •	• •	, ,	
C(21)	3254(23)	2773(5)	, ,	• •
C(20C) C(20D) C(20E)	3196(25) 7800(24) 2797(22)	-1091(5) -487(5) 1938(5)	2390(5) 2397(5) 2590(4) 720(4)	24(5) 19(5) 15(4) 18(4)

Table 4A (Cont'd).

Table 4A (Co	ont uj.			
C(21A)	3532(23)	5800(5)	650(4)	22(5)
C(21B)	11301(23)	4288(5)	772(5)	19(4)
C(21C)	1595(25)	-1308(5)	2436(5)	21(5)
C(21D)	6240(24)	-226(5)	2397(5)	17(5)
C(21E)	1208(25)	1716(5)	2526(5)	20(5)
C(22)	3976(22)	2821(4)	435(4)	7(4)
C(22A)	4178(25)	5540(5)	404(5)	24(5)
C(22B)	10474(24)	4171(5)	494(4)	19(4)
C(22C)	636(26)	-1262(5)	2720(5)	24(5)
C(22D)	5383(23)	-109(5)	2676(4)	15(4)
C(22E)	372(23)	1481(5)	2771(4)	16(4)
O(101)	11073(21)	2215(4)	-160(4)	51(5)
C(102)	11709(62)	2169(13)	-456(11)	166(17)
C(103)	10620(40)	2352(8)	-631(7)	81(9)
C(104)	12281(39)	1722(9)	-489(8)	92(10)
C(105)	12830(63)	1636(15)	-146(12)	182(19)
C(106)	12106(32)	1890(7)	92(6)	59(7)
O(201)	8745(13)	5861(3)	-110(3)	36(2)
C(202)	8076(40)	5866(9)	-412(8)	95(9)
C(203)	8911(37)	5611(8)	-628(7)	71(8)
C(204)	7655(42)	6308(9)	-482(8)	97(11)
C(205)	7179(71)	6480(16)	-140(14)	83(23)
C(206)	7793(27)	6181(5)	71(5)	33(5)
O(301)	5862(20)	1848(4)	3254(4)	60(5)
C(302)	6519(36)	1847(8)	3570(7)	67(8)
C(303)	5345(34)	1693(7)	3783(6)	66(8)
C(304)	7235(32)	2306(7)	3603(6)	56(7)
C(305)	7876(44)	2406(10)	3279(8)	101(11)
C(306)	6802(29)	2158(6)	3064(6)	48(6)
O(401)	1368(26)	3303(6)	3424(5)	103(7)
C(402)	2562(68)	2927(16)	3274(13)	164(23)
C(403)	2193(48)	2868(10)	3062(10)	118(12)
C(404)	2276(34)	2694(7)	3644(7)	70(8)
C(405)	1160(66)	3035(16)	3834(12)	199(21)
C(406)	1302(48)	3448(11)	3774(9)	121(12)

**Table 5A** Atomic Coordinates and Isotropic Displacement Parameters for Rb<sup>+</sup>(Dibenzo[a,c]phenazine)<sup>-</sup>.

	х	у	Z	U(eq)
Rb(1)	1209(1)	1474(1)	2729(1)	33(1)
N(1)	-469(1)	278(3)	2199(1)	22(1)
C(2)	-648(1)	1230(3)	1735(1)	19(1)
C(3)	-110(1)	1009(3)	1243(1)	20(1)
C(4)	551(2)	-170(3)	1248(1)	25(1)
C(5)	1094(2)	-301(4)	797(1)	28(1)
C(6)	996(2)	738(4)	333(1)	29(1)
C(7)	342(2)	1862(3)	313(1)	24(1)
C(8)	-225(1)	2031(3)	761(1)	20(1)
C(9)	-920(2)	3206(3)	740(1)	20(1)
C(10)	-1124(2)	4123(4)	250(1)	27(1)
C(11)	-1802(2)	5175(3)	230(1)	30(1)
C(12)	-2311(2)	5376(3)	701(1)	29(1)
C(13)	-2139(2)	4509(3)	1189(1)	24(1)
C(14)	-1445(1)	3402(3)	1218(1)	19(1)
C(15)	-1296(1)	2424(3)	1725(1)	18(1)
N(16)	-1808(1)	2716(3)	2178(1)	22(1)
C(17)	-1635(2)	1777(3)	2650(1)	21(1)
C(18)	-2119(2)	2015(3)	3140(1)	26(1)
C(19)	-1956(2)	1103(3)	3624(1)	28(1)
C(20)	-1300(2)	-36(3)	3640(1)	28(1)
C(21)	-806(2)	-288(3)	3165(1)	24(1)
C(22)	-971(2)	586(3)	2661(1)	21(1)

#### References

- 1. Miller, J. S.; Epstein, A. J. Angew. Chem. Int. Engl. 1994, 33, 385-415.
- 2. Dougherty, D. A. Acc. Chem. Res. 1991, 24, 88-94.
- 3. Hoffmann, R.; Van Dire, G. W.; Zeiss, G. D. J. Am. Chem. Soc. 1968, 90, 1485-1499
- 4. (a) Hoffmann, R. Acc. Chem. Res. 1971, 4, 1-9. (b) Hoffmann, R. J. Am. Chem. Soc. 1968, 90, 1475-1485-1499.
- 5. Ovchinnikov, A. A. Theor. Chim Acta 1978, 47, 297-301
- (a) Borden, W. T.; Davidson, E. R.; Feller, D.; Kato, S. D.; Morokuma, K. J. Am. Chem. Soc. 1983, 105, 1791-1795.
   (b) Borden, W. T.; Fort, R.C., Jr.; Hrovat, D. A.; Lahti, P. M. J. Am. Chem. Soc. 1992, 114, 7549-7552.
- 7. Clites, J. A.; Dougherty, D. A.; Jacobs, S. J.; Murray, M.; Shultz, D. A.; Silverman, S. K.; West, A. P. *Mol. Cryst. Liq. Cryst.* **1993**, 232, 289-304.
- 8. Dougherty, D. A.; Silverman, S. K.; West, A. P., Jr. J. Am. Chem. Soc. 1996, 118, 1452-1463.
- 9. McConnell, H. M. J. Chem. Phys. 1963, 39, 1910.
- 10. (a) Iwamura, H.; Izuoka, A.; Sugawara, T. J. Am Chem. Soc. 1985, 107, 1786-1787.
- (a) Buchachenko, A.L. *Usp. Khim.* 1990, 59, 529-546. (b) Epstein, A. J.; Miller, J. S.; Reiff, W. M. *Chem. Rev.* 1988, 88, 201-235. (c) Gatteschi, D.; Laugier, J.; Rey, P.; Zanchini, C. *Inorg. Chem.* 1987, 26, 938-943. (d) Caneschi, A.; Gatteschi, D.; Grand, A.; Laugier, J.; Pardi, L.; Rey, P. *Inorg. Chem.* 1988, 27, 1031-1035 (e) Gelman, A. B.; Ikorsky, V. N.; Ovcharenko, V. I. *Zh. Strukt. Khim.* 1989, 30, 142-145.
- 12. Malinouskaya, S. A.; Musin, N. R.; Schastnev, P. V. *Inorg. Chem.* 1992, 31 4118-4121.
- 13. Bu'Lock, J.D.; Harley-Mason, J. J. Chem. Soc. 1951, 2248-2253
- Conklin, B. J.; Lange, C. W.; Pierpont, C. G. *Inorg Chem.* 1994, 33, 1276-1283. (b)
   McGarvey, B. R.; Ozarowski, A.; Peppe, C.; Tuck, D. G. *J. Am. Chem. Soc.* 1991, 113, 3288-3293.

- 15. (a) Fox, G. A.; Pierpont, C. G. Inorg. Chem. 1992, 31, 3718. (b) Abakumov, G. A.; Bubnov, M. P.; Cherkasov, V. K.; Ellert, O.G.; Rakitin, U. V.; Saf'yanov, U. N; Struchkov, Y. T.; Zakharov, L. N.; Isv. Akad. Nauk SSSR 1992, 2315.
- 16. Gardier, M. G.; Hanson, G. R.; Henderson, M. J.; Lee, F. C.; Raston, C. L. Inorg Chem. 1994, 33, 2456-2461.
- 17 Hirota, N. J. Am. Chem. Soc. 1967, 89, 32-41.
- 18. Bock, H.; Fenske, D.; Goosmann, H.; Herrmann, H. Angew. Chem. Int. Ed Engl. 1988, 27, 1067-1069.
- 19. Bakulin, A.; Gopalan, P.; Jackson, J.E.; Stoudt, S.J. *Inorg. Chem.* 1996, 35, 6614-6621.
- 20. Huang, R.; Jackson, J. E.; Kahr, B.; Misiolek, A. J. Am. Chem. Soc., Chem. Commun., 1996, 2119-2120.
- 21. Dye, J. L.; Huang, R.H.; Huang, S. Z. Ichimura, A. S.; Jackson, J. E.; Szajek, P. L.; Wagner, M. J.; Xie, Q. J. Phys. Chem B. 1998, 102, 11029-11034.
- 22. Glarum, S.H.; Haddon, R. C.; Hebard, A. F.; Murphy, D. W.; Palstra, T. T. M.; Rosseinsky, M. J. *Nature* **1991**, 350, 600-601.
- 23. Dabbagh, G.; Eick, R.H.; Fleming, R. M.; Glarum, S.H.; Haddon, R. C.; Hebard, A. F.; Kortan, A. R.; Makhija, A. V.; Miller, B.; Muller, A. J.; Murphy, D. W.; Rosamilia, J. M.; Rosseinsky, M. J.; Tycko, R.; Zaharak, S. M. *Nature* 1991, 350, 320-322.
- 24. Diederich, F.; Holczer, K.; Huang, S.-M.; Kaner, R.; Mihaly, L.; Stephens, P. W. *Nature* 1991, 351, 632-634.
- 25. Coustel, N.; Cox, D. E.; Fischer, J. E.; Kycia, S.; McCauley Jr., J. P.; McGhie, A, R.; Romanow, W. J.; Smith, A. B.; Zhou, O. *Nature* 1991, 351, 462-464.
- 26. Chen, C.-C.; Kelty, S. P.; Lieber, C. M. Nature 1991, 352, 223-224.
- 27. Ebbesen, T. W.; Kubo, Y.; Kuroshima, S.; Mizuki, J.; Saito, S.; Tanigaki, K. *Nature* 1991, 353, 222-223.
- 28. Atherton, N. M.; Weissman, S. I. J. Am. Chem. Soc. 1961, 83, 1330-1334.
- 29. Herold, B. J.; Neiva Correia, A. F.; dos Santos Veiga, J. J. Am. Chem. Soc. 1965, 87 2661-2665.

- 30. Fischer, D.; Gerson, F.; Merstetter, P.; Mlynek, C. J. Am. Chem. Soc. 1998, 120, 4815-4824.
- 31. Andreas, J.; Bock, H.; Nather, C.; Ruppert, K. Helv. Chim Acta 1994, 77, 1505-1519.
- 32. For reviews on alkali metal organic compounds see: (a) Arad, C.; Bock, H.; Gobel, I.; Havlas, Z.; Meuret, J.; Herrmann, H.-F.; Nather, C.; Nick, S.; Rauschenback, A.; Ruppert, K.; Seitz.; Solouki, B.; Vaupel, T. Angew. Chem, Int. Ed. Engl. 1992, 31, 550-581. (b) Schade, C.; Schleyer, P. v. R. Adv. Organomet. Chem. 1987, 27, 169-186.
- 33. Bock, H.; Hauk, T.; Havlas, Z.; Nather, C. Organomet. 1998, 17, 4707-4715.
- 34. Bock, H.; Ruppert, K. Inorg. Chem. 1992, 31, 5094-5099.
- 35. Habich A.; Hausser, K., A.; Franzen, Z. Naturforsch., Teil A 1961, 16, 836-845.
- 36. Maki, A. H.; Stone, E. W. J. Chem. Phys. 1963, 39, 1635-1642.
- 37. Sevenster, A. L.; Tabrer, B. J. J. Org. Mag. Res. 1984, 22, 521-526.
- 38. Carter, H. V.; McClelland, B. J.; Warhurst, E. *Trans. Faraday Soc.* 1960, 56, 455-458.
- 39. Buschov, K. H. J.; Dieleman, J.; Hoijtink, G. J. J. Chem. Phys. 1965, 42, 1993-1999
- 40. Bleaney, B.; Bowers, K. D. Proc. R. Soc. London, Ser. A. 1952, 214, 451.